Planetary Radio Interferometry and Doppler Experiment (PRIDE) Applications to Orbiters and Landers

Klindžić, Dora

UNIVERSITY OF ZAGREB
FACULTY OF SCIENCE
DEPARTMENT OF PHYSICS

Dora Klindžić

PLANETARY RADIO INTERFEROMETRY AND DOPPLER EXPERIMENT (PRIDE) APPLICATIONS TO ORBITERS AND LANDERS

Master Thesis

Zagreb, 2018

SVEUČILIŠTE U ZAGREBU
PRIRODOSLOVNO-MATEMATIČKI FAKULTET
FIZIČKI ODSJEK

Dora Klindžić

PRIMJENE PLANETARNOG RADIO INTERFEROMETRIJSKOG I DOPPLEROVOG EKSPERIMENTA (PRIDE) NA ORBITERE I SLETAČE

Diplomski rad

Zagreb, 2018

UNIVERSITY OF ZAGREB
FACULTY OF SCIENCE
DEPARTMENT OF PHYSICS

INTEGRATED UNDERGRADUATE AND GRADUATE UNIVERSITY
PROGRAMME IN PHYSICS

Dora Klindžić

Master Thesis

Planetary Radio Interferometry and Doppler Experiment (PRIDE) Applications to Orbiters and Landers

Advisor: Vernesa Smolčić, PhD

Co-Advisor: Leonid Gurvits, PhD

Master Thesis grade: _____

Committee: 1. _____

2. _____

3. _____

Master Thesis defence date: _____

Zagreb, 2018

Acknowledgements

The author would like to express her gratitude to her supervisors, Leonid Gurvits of the Joint Institute for VLBI ERIC and Vernesa Smolčić of the Department of Physics at the University of Zagreb for their invaluable knowledge, inspiring passion for research and generous dedication of their time over the course of the past year. This work would not have been possible without their guidance and encouragement. Special thanks are in order for colleagues from JIVE's Space Science and Innovative Applications (SpaSIA) group, Tatiana Bocanegra-Bahamón and Giuseppe Cimó for their insight and assistance, as well as their continuing spirit of teamwork and support.

This Thesis was enabled by an Erasmus+ grant during the author's internship at JIVE from October 2017 to May 2018, which was brought to reality thanks to L. Gurvits. Besides an immensely valuable learning environment, JIVE has proved to be a welcoming community and a source of lifelong connections, many happy memories and fruitful collaborations to come.

The author owes gratitude to all her Professors at the University of Zagreb, especially her previous mentors Vibor Jelić and Nikola Poljak, who have shaped her into a scientist over the course of five years, and to her closest peers, Mateo, Fran, Lovro and Arian, who have shared this path with her and whose accomplishments she will be proud to follow.

Finally, thanks to the Student's Office staff for accomodating the numerous special paperwork requests inside or outside of working hours, and to all the family and friends who had belief in the author's abilities even when she had none.

This work is for all of you.

Primjene Planetarnog Radio Interferometrijskog i Dopplerovog Eksperimenta (PRIDE) na orbitere i sletače

Sažetak

PRIDE: Planetary Radio Interferometry and Doppler Experiment (Duev et al. 2012) inicijativu pokrenuo je Joint Institute for VLBI ERIC (JIVE) s ciljem ultra-preciznog mjerenja vektora stanja svemirskih letjelica (njihovih prostornih koordinata i brzina) kao funkcije vremena, koristeći fazno referenciranu dugobazičnu interferometriju (VLBI) i radijalna Doppler mjerenja. Ova je metoda primjenjiva na bilo koju letjelicu s radioemiterom, a rezultati imaju bogatstvo primjena u disciplinama od planetarne znanosti do visokoprecizne nebeske mehanike, gravimetrije i fundamentalne fizike. Ovaj Rad uključuje pregled postupka planiranja buduće PRIDE opservacije za dvije trenutno aktivne letjelice u Marsovoj orbiti koristeći European VLBI Network (EVN) i Very Long Baseline Array (VLBA) mreže teleskopa, a ujedno i primjer obrade podataka za prethodno izvršen PRIDE eksperiment s Mars Express orbiterom u 2013. godini. Izračunate opservable primijenjene su na radiookultacijsko proučavanje Marsove atmosfere, dajući vertikalne profile refraktivnosti, gustoće, tlaka i temperature. Nadalje, istražene su buduće prilike za primjenu PRIDE-a u okviru potencijalnog eksperimenta s bistatičkim radarom za ESA-inu misiju JUpiter Icy moons Explorer (JUICE), omogućavajući proučavanje površine Jupiterovog mjeseca Europe, kao i primjena na Lander Radioscience (LaRa) eksperiment koji je dizajniran za proučavanje geološke kompozicije Marsove unutrašnjosti. Kvaliteta Doppler podataka s European VLBI Network (EVN) antena usporediva je s Doppler podacima iz zatvorene petlje dobivenim na namjenskim sistemima za praćenje u dubokom svemiru, npr. NASA-in Deep Space Network i ESA-in Estrack (Bocanegra-Bahamón et al. 2018), što ukazuje da PRIDE podaci mogu obogatiti znanstvene rezultate misija koje nisu inicijalno dizajnirane za radioeksperimente.

Ključne riječi: radio astronomija – interferometrija – VLBI – PRIDE – svemirske misije

Planetary Radio Interferometry and Doppler Experiment (PRIDE) Applications to Orbiters and Landers

Abstract

PRIDE: the Planetary Radio Interferometry and Doppler Experiment (Duev et al. 2012) is an initiative by the Joint Institute for VLBI ERIC (JIVE) providing ultra-precise estimates of spacecraft state vectors (spatial coordinates and velocities) as a function of time, utilizing phase-referenced Very Long Baseline Interferometry (VLBI) tracking and radial Doppler measurements. This method is applicable to any radio-emitting spacecraft, and the results can be used in a plethora of disciplines from planetary science to high-precision celestial mechanics, gravimetry and fundamental physics. This Thesis includes an overview of the scheduling procedure for a future PRIDE observation of two active spacecraft in Mars' orbit, involving the European VLBI Network (EVN) and Very Long Baseline Array (VLBA) telescopes, as well as a demonstration of the data processing pipeline for a PRIDE experiment performed with the Mars Express orbiter in 2013. The resulting observables are applied to a radio occultation study of the Martian atmosphere, yielding vertical refractivity, density, pressure and temperature parameters. Furthermore, future opportunities for PRIDE are investigated in terms of a potential bistatic radar experiment with ESA's JUpiter Icy moons Explorer (JUICE) mission, enabling a study of the surface of the Jovian moon Europa, as well as applications to the Lander Radioscience (LaRa) experiment which is designed to study the geological composition of Mars' interior. The quality of the Doppler data from the single European VLBI Network (EVN) antennas is comparable to closed-loop Doppler data obtained by dedicated deep space tracking systems like NASA's Deep Space Network and ESA's Estrack (Bocanegra-Bahamón et al. 2018), proving that PRIDE data could enhance the science return of missions not initially designed for radio science experiments.

Keywords: Radio astronomy – Interferometry – VLBI – PRIDE – Space missions

Contents

1 Introduction

Precision has always been a determining factor in the successes and failures of space missions. In a branch of experimental science where costs are measured in billions of Euros and mission opportunities average at $\sim$2 per career lifetime, the margin of error must be absolutely minimal. For obtaining this goal, space science and technology has reached for an interdisciplinary alliance with radio astronomy; in particular the method of *Very Long Baseline Interferometry (VLBI)*, an astronomical technique of unprecedented precision with a plethora of applications. The Netherlands-based Joint Institute for VLBI ERIC[1] (JIVE) has created an initiative for radioastronomical enhancement of planetary missions' science return named the *Planetary Radio Interferometry and Doppler Experiment (PRIDE)*, the applications of which to ongoing and future planetary missions shall be discussed in this thesis.

1.1 Very Long Baseline Interferometry (VLBI)

The first application of interferometry in astronomy dates back to Michelson's stellar interferometer (1890 - 1920), an optical double-slit experiment which enabled an estimation of stellar diameter for several brightest stars. The increase in resolution required to make this experiment possible results from the fact that a single aperture of diameter d has an angular resolution $\theta \sim \lambda/d$, but two such apertures separated by a large distance D form a fringe pattern with improved resolution $\theta \sim \lambda/D$. Several decades after Karl Jansky's historic discovery of cosmic radio emission in 1933, radio astronomers and physicists realized the applicability of interferometry to the newborn practice of radio astronomy. Considering the large wavelength of radio waves, the angular resolution of a single radio telescope dish was quite poor. Applying the learnings from the optical counterpart, the first two-element radio interferometer performed its observations in 1946. A new vocabulary had entered radioastronomical discourse: concepts such as baseline, fringe and geometric delay became crucial for interpreting the new observations.

A sketch of this simple two-element interferometer is seen in Fig. 1.1. A point source in the direction of unit vector $\hat{s}$ is emitting monochromatic radiation of fre-

[1] "ERIC" stands for European Research Infrastructure Consortium. The principal task of an ERIC is to establish and operate new or existing research infrastructures on a non-economic basis.

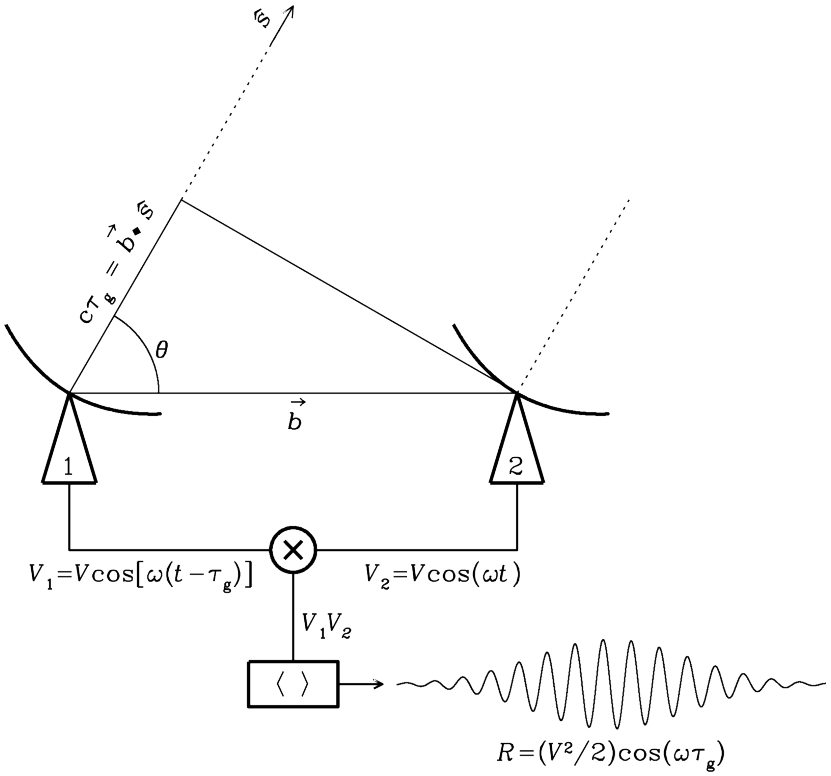

Figure 1.1: A diagram of the components of a two-element interferometer. Vector $\hat{s}$ points towards the target source, $\vec{b}$ is the baseline. Output voltages V_1 and V_2 are multiplied and averaged by the correlator, creating a time-dependent interferometric fringe. (Source: NRAO)

quency $\nu = \omega/(2\pi)$. The vector pointing from antenna 1 to antenna 2 is the *baseline* vector. The length of the projection of the baseline vector on the image plane will determine the angular resolution of this configuration. Incident radiation will produce output voltages at the two receivers, retarded by the *geometric delay* $\tau_g = \vec{b}\cdot\hat{s}/c$. These voltages are amplified, multiplied ($\times$), and time averaged ($\langle\rangle$) by a device called the *correlator* (because the time average of the product of two signals is proportional to their cross-correlation), generating an output *fringe* which varies as

$$R = \frac{V^2}{2}\cos(\omega\tau_g) = \frac{V^2}{2}\cos\left(\frac{\omega b}{c}\cos\theta\right). \tag{1.1}$$

The amplitude of this response is proportional to the flux density of the point source, and the phase depends on the position of the source in the sky. The broad Gaussian envelope of the fringe shown in Fig. 1.1 shows how the quasi-sinusoidal signal is attenuated as the source passes through the beam of the dishes as their pointing remains fixed.

Evidently, a small shift dθ in the position of the source registers as a fringe phase

shift

$$\mathrm{d}\phi = \frac{\omega b}{c} \sin\theta \, \mathrm{d}\theta. \tag{1.2}$$

The fringe phase is thus an exquisitely sensitive measure of source position if the projection of the baseline $b \sin\theta$ is many wavelengths long. Using highly precise atomic clocks in measuring the fringe phase, one can obtain sub-arcsecond precision in measurements by ensuring coherence in the two received data streams (signals). This realization prompted the first fully successful VLBI experiment to be conducted a little over 50 years ago, in 1967. It included stations at the Algonquin Radio Observatory near Ottawa, Ontario, and the Dominion Radio Astrophysical Observatory near Penticton, British Columbia, a baseline of impressive 3,074 kilometers (Broten et al. 1967). What set VLBI apart from conventional radiointerferometry is nonexistence of physical connection between interferometer elements, rendering real-time data processing impossible. Observations had to be recorded on tape and timestamped with utmost precision, then transported to a facility which would correlate and process the data.

The next development in interferometry was adding multiple (N) telescopes to an interferometer, thus creating $N(N-1)/2$ simultaneously observing baselines (resulting in a wider range of observed spatial scales), and increasing the total collecting area (resulting in higher sensitivity). Furthermore, if the observing times were made to be very long, rotation of the Earth would cause baseline projection lengths to vary with respect to the source, increasing the range of possible baseline lengths even further. However, with the creation of increasingly complex multi-element interferometric arrays, imaging also became more complicated. New methods had to be developed using Fourier analysis, which are now known as *aperture synthesis* (Ryle 1961). Essentially, this procedure allows us to reconstruct the image produced by any given telescope aperture by only sampling the cross-correlation of the radiation field at a given set of points on the aperture. If we now consider our array as one giant aperture with radius corresponding to the longest baseline, we can synthesize an image as seen by this imaginary giant telescope just from the output of individual pairs of telescopes. The quality of this image depends on the number and variation of baselines, as it increases the completeness of the Fourier space.

(For a more comprehensive overview of the history of radio interferometry and

the mathematics behind aperture synthesis, see textbooks by Thompson et al. (2017) or Wilson et al. (2009).)

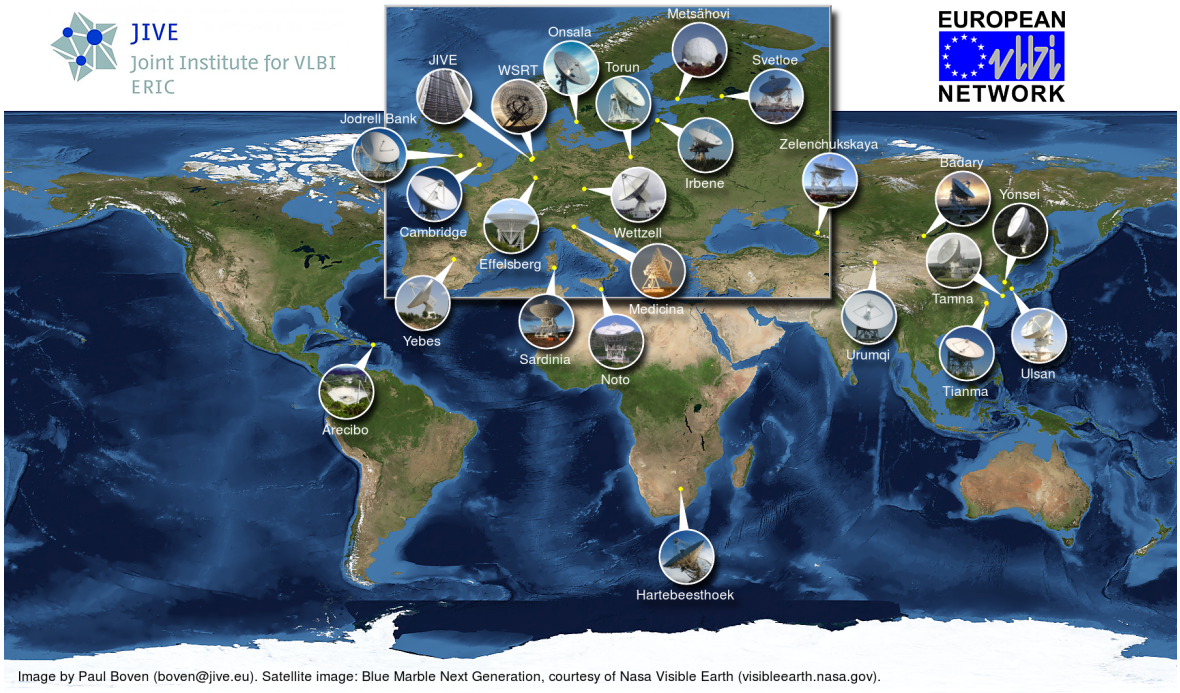

Figure 1.2: A global map of European VLBI Network telescopes as of December 2016. (Courtesy of P. Boven.)

In the case of modern VLBI, this synthesized aperture can have the diameter of the Earth, or even larger if radio observing satellites are included. Institutes like JIVE are tasked with coordinating observations using a network of international, globally distributed individual telescopes, most notably the *European VLBI Network (EVN)*. The EVN is a network of radio telescopes located primarily in Europe and Asia, with additional antennas in South Africa and Puerto Rico, having the ability to perform high angular resolution observations of cosmic radio sources. (See map in Figure 1.2.) For reference, the milliarcsecond resolution obtainable by the EVN is a hundred times better than the resolution of the optical Hubble telescope. It is the most sensitive VLBI array in the world, thanks to the collection of extremely large telescopes that contribute to the network. Global VLBI observations are also often conducted in conjunction with the Very Long Baseline Array (Fig.1.3) in the USA and the Russian RadioAstron satellite in Earth orbit.

The data processing for the EVN is also done at JIVE; observations were historically recorded on high capacity magnetic tapes at individual telescopes, and these are later replayed and combined at a special purpose data processor - the “Correlator”

Figure 1.3: A map of Very Long Baseline Array telescopes. (Credit: NASA's Goddard Space Flight Center)

- a supercomputer located at the JIVE headquarters in Dwingeloo, the Netherlands. Nowadays, the data is stored on specialized hard drives, but advances in optical fibre technology have recently inspired the development of *e-VLBI* (Garrett 2004), a novel technique in which VLBI streams are transmitted to the JIVE Correlator in real time even from the most remote stations across the world, paving the way for the next generation of radio astronomy free of the need for physical delivery of recordings.

1.2 Planetary Radio Interferometry and Doppler Experiment (PRIDE)

This research applies the methods of VLBI somewhat unconventionally. Instead of observing radio signals of distant galactic and extragalactic sources, we observe the transmissions of spacecraft within the Solar System.

PRIDE: the Planetary Radio Interferometry and Doppler Experiment (Duev et al. 2012) is an initiative by the Joint Institute for VLBI ERIC (JIVE) providing ultra-precise estimates of spacecraft state vectors (spatial coordinates and velocities) as a function of time utilizing phase-referenced[2] VLBI tracking and radial Doppler mea-

[2]*Phase referencing* is the technique of observing angularly nearby calibrator sources of known properties to correct for atmospheric effects during observation of a target.

surements. This method is applicable to any radio-emitting spacecraft, and the results can be used in a plethora of disciplines from planetary science to high-precision celestial mechanics, gravimetry and fundamental physics. Although PRIDE shares some similarities with traditional astrometric applications of the VLBI technique, additional modifications are required in the data processing stage to account for the spacecraft emitting in the near-field regime of the VLBI-synthesized aperture. These are not simple corrections, as the incoming radiation can no longer be treated in the plane-wave approximation. For this purpose, a dedicated software toolkit has been developed at JIVE. In addition to the VLBI observables, PRIDE can also produce open-loop radial Doppler observables for the spacecraft by processing data from individual telescopes separately.

This "open-loop" characteristic of PRIDE is what sets it apart from conventional "closed-loop" tracking methods employed by NASA's Deep Space Network or ESA's Estrack (Kinman 1992). Essentially, in traditional two-way Doppler closed-loop mode (Fig.1.4), the ground station transmits an uplink generated by an ultra-stable oscillator (a hydrogen maser clock) which is then received by the spacecraft using a narrow bandpass filter, the so-called Phase-Locked-Loop. The spacecraft uses this uplink as a stable frequency reference, multiplies it by the transponder ratio (a ratio of integers) and retransmits a downlink signal. The ground station then applies a similar Phase-Locked-Loop to predict the frequency at which the signal should be received and then aligns its passband to (establishes lock with, or tracks) the received signal in real time. This mode of tracking is crucial for mission operations where near-real time reconstruction of the spacecraft state vector is key. However, should the spacecraft signal vary abruptly, the closed-loop station will fall out of lock. This is where the open-loop mechanism of PRIDE offers improved performance in "shadow-tracking" mode, by observing the downlink without participating in the uplink. In the open-loop case, the ground station does not utilize the PLL method of adjusting its passband and instead records the signal on a wide bandwidth channel which does not change over time, as in typical radio astronomical observations. No real time tracking of the spacecraft can be performed without the PLL, but the spacecraft state vector can be reconstructed in postprocessing (as described in Subsection 3.3) with increased precision even in cases where a closed-loop system would have lost the lock on the signal.

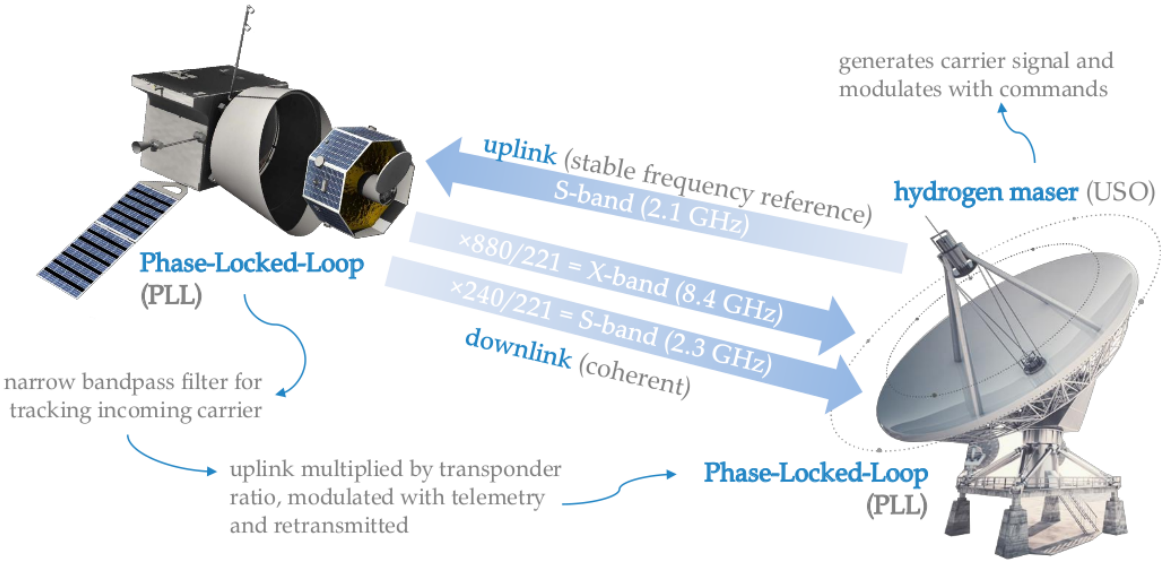

Figure 1.4: A schematic of traditional two-way dual-frequency closed-loop Doppler tracking of spacecraft (in this Figure, ESA's BepiColombo).

The accuracy of the PRIDE method was first demonstrated by Duev et al. (2012) by tracking ESA's Venus Express spacecraft under the EVN observing project EM081. Despite unfavourable observing conditions (low target declination, high separation with calibrator), the orbit accuracy estimate was at a 3-sigma level of 200-300 m across the VEX track and 500-600 m along the track. A significant sharpening of the PRIDE technique was achieved by tracking MEX during its closest fly-by of Phobos under the EVN experiment GR035 (Duev et al. 2016), enabling the measurement of the lateral position and radial Doppler of the MEX spacecraft with a precision of about 50 m and 30 μm/s, respectively. These results are comparable to closed-loop Doppler data obtained by dedicated deep space tracking systems like NASA's Deep Space Network and ESA's Estrack (Bocanegra-Bahamón et al. 2018), proving that PRIDE data could enhance the science return of missions not initially designed for radio science experiments. As such, PRIDE has been selected by ESA to provide high-precision tracking for the JUpiter ICy moons Explorer mission (JUICE) launching in 2022.

Many other opportunities for the application of PRIDE are possible both in existing and future missions. However, the precision of PRIDE depends heavily on the availability of a nearby phase calibrator source; that is, a compact unresolved radio source of known spectral properties (most commonly a quasar) which is observed by the telescopes to remove the effects of atmospheric interference and instrumental

phase. If the nearest calibrator is too far from the target, atmospheric conditions might vary at this scale, resulting in poor image quality. If the calibrator is within 2^o of the target, calibration can be performed, but the telescopes have to be periodically steered back-and-forth between the target and calibrator, a practice known as *nodding*. Ideally, the phase reference source and the target should be within the primary beam of the largest telescope in the VLBI array, in which case both sources can be observed simultaneously by all the telescopes, yielding results of the highest quality.

These considerations greatly impact mission and observation planning, so the focus of the following chapter is on describing the steps necessary for scheduling, planning and preparation for a PRIDE observation for two currently ongoing Martian missions.

2 Scheduling a PRIDE observation

Before a PRIDE observation can be conducted, it is necessary to consider many factors: spacecraft transmission windows, in-beam phase-referencing opportunities with a nearby calibrator, observing station availability, etc. This section presents an overview of the scheduling process for a future PRIDE opportunity.

2.1 A dual-spacecraft PRIDE experiment

The increasing number of artificial satellites in Mars orbit is a testament to the wealth of scientific insight gained from continuous studies of our most Earth-like planetary neighbour. Out of six currently active orbiters in the Martian system, two are operated by the European Space Agency (Fig.2.1): Mars Express (Schmidt 2003) and the ExoMars Trace Gas Orbiter (Gibney 2016). This offers a unique opportunity to observe transmissions from both spacecraft simultaneously.

Mars Express (MEX) was Europe's first mission to Mars, an international effort including a stereoscopic camera from Germany, a mineralogical mapping device from France and an atmospheric sounder from Italy. Efforts were joined with the Jet Propulsion Laboratory in California to engineer a radar probe for subsurface water, and with the UK for the construction of the accompanying Beagle-2 lander. Launched in 2003, its impressive science return has justified six mission extensions, lengthening the lifespan of the durable orbiter well into its second decade. MEX has since become an invaluable communications relay between landers on the Martian surface and Earth, transmitting a downlink signal at X-band (8.4 GHz). MEX has been the favourite target of the Space Science and Innovative Applications group at JIVE for many years. Analysis of its signal allowed them to characterize the solar wind, including the study of a Coronal Mass Ejection (Molera Calvés 2017). Observed for over a decade, it has served as a prototype study for the Planetary Radio Interferometry and Doppler Experiment (PRIDE).

In October 2016, the *ExoMars Trace Gas Orbiter* (TGO), a collaboration between ESA and Russian Roscosmos, was successfully injected into Mars orbit. The TGO is a hybrid science and telecom orbiter tasked with analyzing the Red Planet's atmosphere for traces of methane and other atmospheric signatures of biological activity, as well as providing a communications link for upcoming surface missions such as the 2020

ExoMars rover. The TGO has completed its aerobraking procedure in March 2018 and settled into a 400 km circular orbit, where it will perform its science operations.

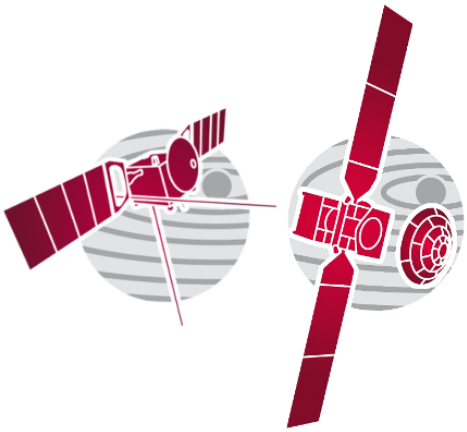

Figure 2.1: Mission insignia for Mars Express (left) and ExoMars 2016 (right), consisting of the Trace Gas Orbiter and Schiaparelli lander. (Copyright: ESA)

High-precision reconstruction of MEX's orbit during the Phobos fly-by in 2013 enabled the gravitational field of Phobos to be studied, shedding light on the moon's internal geological composition and in turn its mysterious origin. Now, the presence of two simultaneously transmitting spacecraft in Mars orbit offers an opportunity for a dual PRIDE experiment, resulting in twice the science return at the cost of one observation (an equivalent of 'two birds with one stone'). The resulting data could theoretically be used to better constrain the ephemeris (trajectory) of Mars, as well as providing a valuable case study for future PRIDE experiments in the Jovian system. In the following subsection, we will explore potential observing opportunities for this experiment to be conducted.

2.2 The search for phase calibrators

As mentioned earlier, the precision of a PRIDE observation depends on the availability of a calibrator (phase reference) source in the immediate vicinity of the target source. Considering that our target is a planet, or rather the spacecraft in its orbit, the target significantly travels across the celestial background relative to distant extragalactic radio sources over the course of several hours. Therefore, the first step is to generate a *finding chart*: a list (or plot) of the coordinates of Mars in the sky for a given time period as observed from Earth.

The motion of planets is a highly complex numerical integration of an n-body

problem, involving perturbational effects due to the interaction of all Solar System bodies, tidal forces, libration, relativistic corrections and many more considerations. To generate the ephemeris of Mars, we will use the Jet Propulsion Laboratory Development Ephemeris DE432s (Folkner et al. 2014), the latest model of the Solar System produced at the Jet Propulsion Laboratory in Pasadena, California, primarily for purposes of spacecraft navigation and astronomy. The model consists of computer representations of positions, velocities and accelerations of major Solar System bodies.

The JPL ephemerides are accessed through `astropy`, a community Python package for astronomy. The observing location is set to Greenwich, the default, as it will not significantly impact the ephemeris at the arcminute scale. The ephemeris of Mars is computed in GCRS[3] for the time range of 25th October 2017 to 1st October 2019, sufficient time for the it to wrap fully around the celestial sphere.

The next step is to form a strip of sky two degrees wide, centered on the ephemeris, and to look for radio sources within this strip. These sources could all be used as potential calibrators for the PRIDE experiment if the telescopes are set to nodding mode.

We perform a coordinate search in the Radio Fundamental Catalogue (RFC) (Petrov 2017), currently the most complete catalogue of compact radio sources produced by analysis of all available very long baseline interferometry (VLBI) observations under absolute astrometry and geodesy programs since year 1980. It contains precise positions with milliarcsecond accuracies for 14,786 objects.

The resulting 278 potential calibrators are shown in red in the finding chart in Figure 2.2. We find that they are more or less uniformly distributed along the ephemeris. Now we wish to further constrain the angular separation between Mars and the calibrators to 2 arcminutes, seeking opportunities for in-beam observations.

The instances of near-passes at less than 2 arcminute separation are listed in Table 2.1. The RFC coordinates were cross-checked with the NASA Extragalactic Database (NED) through the `astroquery` package to provide additional information about the sources. We are presented with 5 observing opportunities for an in-beam dual-spacecraft PRIDE experiment.

However, only the first of these events coincides with the Standard EVN observing

[3]The Geocentric Celestial Reference System.

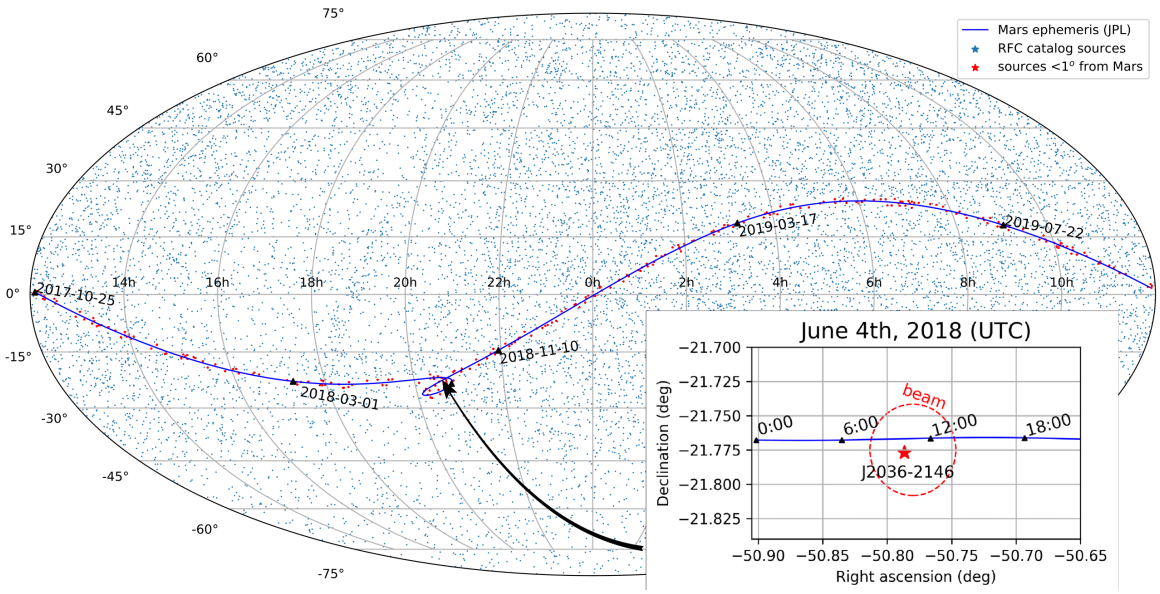

Figure 2.2: A finding chart for Mars for the time period of 25th October 2017 to 1st October 2019 displayed in the Mollweide projection. The ephemeris is plotted in blue and timestamped (YYYY-MM-DD), Radio Fundamental Catalogue sources are marked with blue stars, potential calibrators are marked with red. The inset shows an in-beam phase-referenced observing opportunity on June 4th, 2018. The beam width is set to 4 arcminutes.

Table 2.1: **Potential in-beam phase reference sources**

RFC name	RA (h:m:s)	dec (d:m:s)	NED name	near pass date
J2036−2146	20:36:51	−21:46:36	LQAC 309-021 001	2018-06-04
J2033−2253	20:33:16	−22:53:17	PKS 2030-23	2018-09-29
J2247−0850	22:47:52	−08:50:22	WISE J224752.19-085022.0	2018-12-02
J0033+0335	00:33:12	+03:35:50	GALEXASC J003312.82+033549.7	2019-01-14
J0103+0659	01:03:31	+06:59:21	PMN J0103+0659	2019-01-27

sessions scheduled for this year (Session 2: May 24th – June 14th, as per the EVN Call for Proposals online). Hence, we will focus on planning an EVN observing campaign for June 4th as a pilot project. The remaining dates may all be observed during the Very Long Baseline Array (VLBA) sessions as part of a long-term campaign.

2.3 EVN observation

The pilot observing opportunity on June 4th 2018 will involve source J2036-2146 (Fig.2.3) as an in-beam phase-reference calibrator. A query of NED and Veron-Cetty catalogue reveals this object to be a flat-spectrum[4] radio source classified as a quasar at redshift z=2.299. Integrated flux density at X-band is 229 mJy[5], sufficient to

[4]A spectrum is *flat* if flux density is constant as a function of frequency.
[5]Jansky is a typical radioastronomical unit of spectral flux density, 1Jy = 10^{-26} Wm^{-2}Hz^{-1}.

provide a good signal-to-noise ratio as a calibrator. The source is compact and unresolved with position accuracy of 0.33 mas, which is also a constraint on the accuracy of the spacecraft orbit determination. The position of the calibrator could be further improved with VLBI observations outside of this experiment.

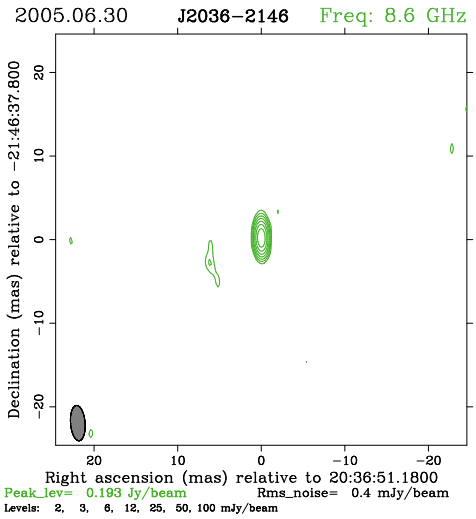

Figure 2.3: A contour map of brightness distribution at X-band for source J2036-2146. (Credit: Yuri Y. Kovalev, astrogeo.org database)

The hourly angular separation between J2036-2146 and Mars on the target date is presented in Table 2.2. A plot of the ephemeris and the calibrator can be seen in the inset in 2.2. Clearly, the in-beam window when the angular separation is less than 4 arcminutes is between 04:00 and 15:00 UTC.

Table 2.2: **Angular separation between Mars and calibrator**

Time (ISO, UTC)	Separation (d:m:s)
04:00	0:03:40.5140
05:00	0:03:04.5339
06:00	0:02:28.8104
07:00	0:01:53.5628
08:00	0:01:19.6930
09:00	0:00:50.8980
10:00	0:00:41.5633
11:00	0:01:02.3625
12:00	0:01:35.9267
13:00	0:02:13.3250
14:00	0:02:52.2992
15:00	0:03:32.0582

The observation will be planned and scheduled using SCHED, the universal program for creation and distribution of schedules to VLBI telescopes and correlators.

Among other things, SCHED can offer useful elevation-time and uptime plots for each of the observing stations. This is crucial in planning the observing time and deciding on the participating telescopes. These plots are shown in Figure 2.4 for our calibrator source and 7 stations (west to east): Yebes (Spain), Effelsberg (Germany), Medicina (Italy), Onsala (Sweden), Wettzell (Germany), Noto (Italy) and Hartebeesthoek (South Africa). Evidently, the low target declination (-21.46^o) is inconvenient for the European stations, as the maximum elevation the source reaches is around 20^o or less, which is not ideal. The source is not visible for other stations during the in-beam window.

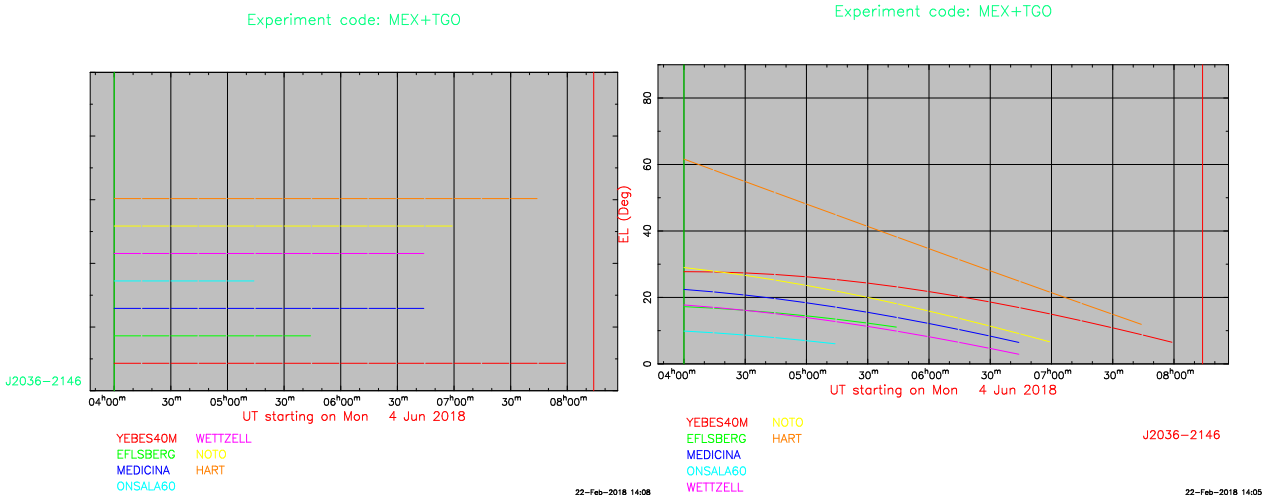

Figure 2.4: SCHED output for uptime per telescope (left) and elevation vs. universal time (right) for target J2036-2146 on June 4th 2018. The 7 telescopes are listed below the image and in the text.

A list of uptimes per station is given in Table 2.3. We can now further eliminate stations from our list, starting with Onsala, because the elevation of the source is unacceptably low. Furthermore, the half-power beam width (HPBW) will be determined by the antenna diameter using formula HPBW [rad] $= \lambda/D$. Since the two spacecraft emit at X-band (8.4 GHz), the waveband of interest is λ=3.6 cm. Evidently, Effelsberg would not be acceptable in our situation if we don‘t permit nodding, because the beam size is smaller than the angular separation between Mars and the calibrator.

This suggests that we should constrain our observing time from 04:00 to 06:00 UTC and use the stations Yebes, Medicina, Wettzell, Noto and Hartebeesthoek, which gives us 10 baselines.

Finally, we need to specify the recording format for the observation, taking into account the transmission specifics of the spacecraft. The observation should be

Table 2.3: **Diameters, beam widths and uptimes (UTC) per antenna for source J2036-2146 during in-beam window on June 4th 2018**

Station	D (m)	BW (")	Rising	Setting
Yebes	40	3.1	04:00	08:14
Effelsberg	100	1.2	04:00	06:14
Medicina	32	3.9	04:00	06:59
Onsala	20	6.2	04:00	05:29
Wettzell	20	6.2	04:00	06:59
Noto	32	3.9	04:00	07:14
Hartebeesthoek	26	4.8	04:00	07:45

recorded in 256 Mbps bitrate in a single polarization at X-band. The polarization should be divided in 4 channels, each 16 MHz wide, all centered on 8420.432 MHz, the telemetry/tracking frequency for MEX and TGO. The wide bandwidth will enable us to detect signals from both spacecraft in the same channel. This information, combined with the scheduling parameters produced by SCHED, completes the setup for an EVN-based PRIDE observation.

The in-beam phase-referencing configuration in this pilot project will enable us to determine absolute positions of the two orbiters with 1 nrad accuracy which, accounting for distance between Earth and Mars on June 4th 2018, translates to about 100 m in Mars orbit. The differential trajectory (i.e. the separation vector between the orbiters) is expected to be accurate to the order of tens of meters, considering nonlinear instrument errors and interference due to ionospheric and solar plasma effects (see Folkner et al. (1993) for a comprehensive error budget estimation). A further improvement of the position of the calibrator could improve the maximum attainable accuracy.

The return from this experiment will provide us with a good basis to handle data from a long-term observing campaign conducted by the VLBA telescopes on the remaining dates listed in Table 2.1.

2.4 VLBA observations

Of the four RFC sources listed in Table 2.1 as potential in-beam calibrators after June 4th, three have very accurately determined properties, whereas J2033−2253 has no X-band flux data in the catalogue and is therefore not suitable as a calibrator. We are left with three observing opportunities within the VLBA Semester 2018B (2018

August 1 – 2019 January 31) as depicted in Figure 2.5. More information about the calibrators is given in Table 2.4.

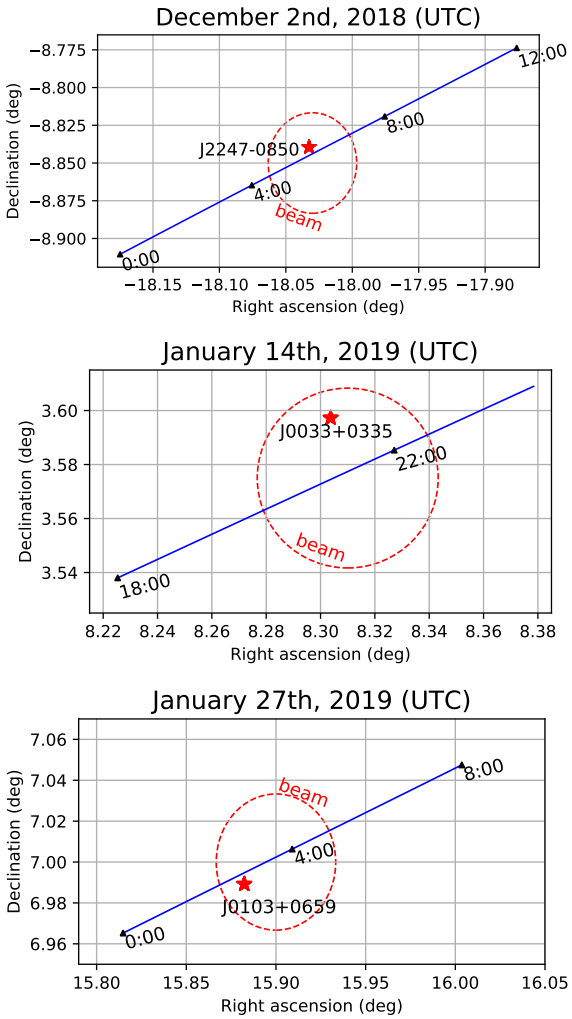

Figure 2.5: A finding chart for Mars for the three target epochs. The ephemeris is plotted in blue and timestamped (UTC) and in-beam phase calibrators are marked with red stars. The beam width is set to 4 arcminutes.

Table 2.4: **Information about the VLBA calibrators**

Source	Date	Min. separation (d:m:s)	Max. sep. (d:m:s)	F_{unr} (Jy)	Positional error (mas)
J2247−0850	2018-12-2	0:00:34	0:03:45	0.061	0.54
J0033+0335	2019-1-14	0:01:25	0:02:56	0.017	1.24
J0103+0659	2019-1-27	0:00:51	0:02:37	0.025	2.60

The optimal observing times for these events were again calculated using SCHED. The in-beam windows are determined by the primary beam width of the 25 m dishes, which is approximately 5 arcmin. Uptimes per antenna within the in-beam windows can be seen in Table 2.5. Fortunately, the sources are visible to the VLBA during all

the in-beam windows, offering us long observing times with up to 10 stations at a time. The technical setup for these observing runs is the same as for the pilot EVN project.

Table 2.5: **In-beam windows (IBW), uptimes in UTC and optimal observing times per VLBA antenna for three in-beam opportunities**

Stations	2nd December 2018 IBW: 03:00 − 08:00	14th January 2019 IBW: 20:00 − 23:00	27th January 2019 IBW: 01:00 − 04:00
Saint Croix	03:00−03:30	20:00−23:00	01:00−02:30
Hancock	03:00−03:15	20:00−23:00	01:00−03:15
North Liberty	03:00−04:45	20:00−23:00	01:00−04:00
Fort Davis	03:00−06:00	20:00−23:00	01:00−04:00
Los Alamos	03:00−06:00	20:00−23:00	01:00−04:00
Kitt Peak	03:00−06:30	20:00−23:00	01:00−04:00
Pie Town	03:00−06:15	20:00−23:00	01:00−04:00
Owens Valley	03:00−06:45	20:00−23:00	01:00−04:00
Brewster	03:00−06:30	20:00−23:00	01:00−04:00
Mauna Kea	03:00−08:00	20:00−22:00	01:00−04:00
Obs. time	03:00−06:30	20:00−23:00	01:00−04:00

This long-term observing campaign will yield data which can be applied to various kinds of planetary science. Firstly, we will obtain three highly accurate determinations of the position of the Martian center of mass (four, counting the EVN pilot) with respect to remote AGNs, thus helping constrain the known Mars orbit, the calculations of which are based mostly on Doppler measurements. Secondly, multiple simultaneous observations of the two orbiting spacecraft, besides having the important role of removing atmospheric and plasma effects, will also allow us to study the gravitational field of Mars. The gravitational field affects the orbital elements for each spacecraft; and whereas most Martian orbiters have a polar orbit (Mars Express included), TGO has an inclination of 70^o, offering an unprecedented insight into the gravity coefficients. We could use this peculiarity to determine the tidal Love number[6] *k2* with higher accuracy.

Besides their relevant science return, these observations will also be a case study for future PRIDE experiments.

[6]The Love numbers are dimensionless parameters that measure the rigidity of a planetary body and the susceptibility of its shape to change in response to a tidal potential.

3 PRIDE example: Atmospheric study of Mars

Using data from a previously performed PRIDE observation of Mars Express on December 28-29 2013, involving more than 30 radio telescopes (European VLBI Network (EVN) / Global VLBI experiment code GR035), we may demonstrate the application of PRIDE data to planetary science purposes; in particular, to atmospheric studies. Considering that the stations have recorded an occultation of the spacecraft signal, i.e. the ingress of the spacecraft behind the visible limb of Mars and its eventual egress, a derivation of vertical pressure, density and temperature profiles for a column of the atmosphere is possible, utilizing the radio occultation pipeline developed for PRIDE by Bocanegra-Bahamón (2018, in prep.).

3.1 Radio occultation method

Radio occultation studies are remote sensing[7] experiments involving a transmitting spacecraft, a planetary body and receiver(s) on Earth. Depending on the viewing geometry, an orbiting spacecraft may undergo an occultation by the central body, which will be directly observable from the (partial or total) loss of the S/C carrier signal generated by the onboard ultra-stable oscillator (USO). The atmosphere and the exosphere of the body in question will make this process gradual: the carrier signal will cut through successively deeper layers of the atmosphere during ingress, undergoing refraction, absorption and scattering which will alter its frequency and amplitude. The same process is observed in reverse upon egress. If the spacecraft state vector is known to sufficiently high accuracy, a predicted Doppler model of the signal in absence of atmospheric effects can be computed and then directly compared to the detected signal, providing information on the planetary atmosphere at the ingress/egress point.

In the interest of obtaining more comprehensive knowledge of a planet's atmosphere, many occultations at various different latitudes and longitudes should be observed. Hence, radio occultation experiments have been performed over the years by multiple spacecraft with varying orbital parameters. An overview of the experiments for Mars, our target of interest, is presented in Table 3.1. These experiments

[7] Remote sensing, unlike on-site observation, is the acquisition of information about a planetary body without physical contact.

are routinely performed with the ESA and NASA Deep Space tracking networks, but it has been demonstrated that the data produced by PRIDE utilizing global VLBI antennas can probe even deeper layers of planetary atmospheres (Bocanegra-Bahamón, 2018, in prep.).

Table 3.1: **History of radio occultation experiments on Mars.**

Spacecraft	Year	No. of occs.	Latitudes (^{o})	References
Mariner IV	1965	1	-50.5,+60	Kliore et al. (1965) Fjeldbo & Eshleman (1968)
Mariner VI & VII	1969	2	+4,+80 -68.2, +38.1	Kliore et al. (1970, 1969) Rasool et al. (1970) Fjeldbo et al. (1970, 1971)
Mariner IX	1971 1972	160	-40 $-$ +20 -80 $-$ +86	Kliore et al. (1972, 1973) Cain et al. (1972, 1973) Weiner & Withers (2013)
Mars 2-6	1972-1976	N/A	N/A	Kolosov et al. (1975) Vasil'Ev et al. (1975) Savich et al. (1976)
Viking 1	1976	N/A	-75 $-$ +70	Fjeldbo et al. (1977)
Viking 2	1979	$\sim$ 100	-74 $-$ +73	Lindal et al. (1979) Simpson & Tyler (1981)
Mars Global Surveyor	1998-2005	$>$21,000	+60 $-$ +85 $\sim$-67	Tyler et al. (2001) Hinson et al. (1999) Noguchi (2012) Cahoy et al. (2006) Cui et al. (2015)
Mars Express	2004 - now	$>$600	-90 $-$ +90	Pätzold et al. (2005) Tellmann et al. (2013) Zhang et al. (2015) Pätzold et al. (2016)
MRO & Odyssey (Cross-link)	2007	3	-20 $-$ +5 -16 $-$ +10	Ao et al. (2015)
Mars Reconnaissance Orbiter	2008 - now	$\sim$180	-90 $-$ +90	Hinson et al. (2012, 2014)

3.2 Geometry and approximations

The occultation geometry is depicted in Figure 3.1, following Fjeldbo et al. (1971). The coordinate system is centered on the target planet and the transmitter and receiver coordinates are marked with subscripts T and R respectively.

The spacecraft signal propagates through different layers of the atmosphere during the occultation event, interacting with the neutral gases and plasma. The refractive index (by which we mean the real part of the complex refractive index, the

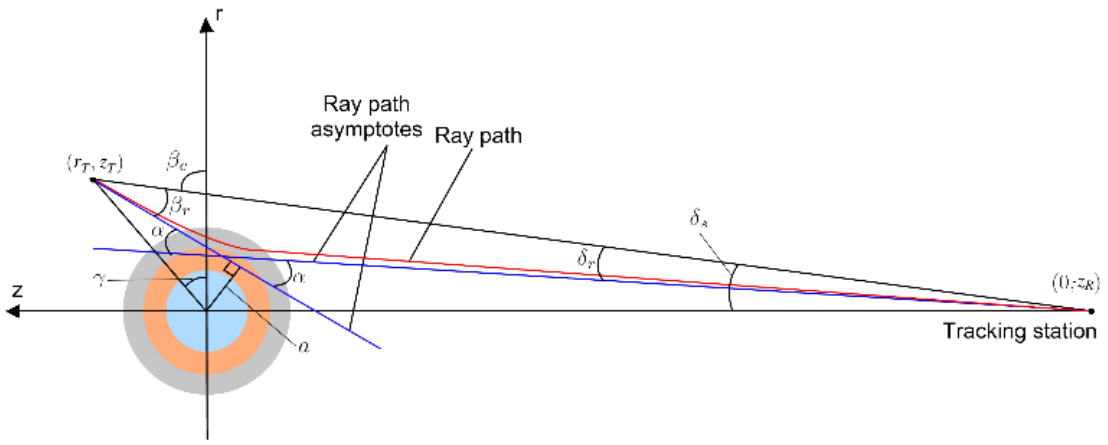

Figure 3.1: Geometry of the radio occultation. The planet's ionosphere (gray) refracts the ray path (red) by an angle α. (Credit: T. Bocanegra)

imaginary part of which we are not interested in as it corresponds to the decrease in amplitude) of this medium varies with altitude, and is proportional to the decrease in signal phase. This corresponds to the measurable frequency changes in the carrier signal.

Assuming that the carrier signal wavelength is smaller than the scales at which atmospheric properties vary, the radio wave can be treated in the classical light ray approximation. By laws of geometric optics, if the atmosphere is modeled as a spherically symmetric medium of refractive index $n(\mathbf{r})$, the ray $\mathbf{r}(s)$ as a function of arclength s satisfies the differential equation (Born & Wolf 1999):

$$\frac{\mathrm{d}}{\mathrm{d}s}\left(n\frac{\mathrm{d}\mathbf{r}}{\mathrm{d}s}\right) = \nabla n. \tag{3.1}$$

In our case, we wish to invert this equation to obtain the refractivity from ray path parameters, in particular the bending angle α and impact parameter a (see Fig.3.1).

What follows is a derivation of these ray path parameters from the Doppler shift of the real received spacecraft signal with respect to a prediction of the received frequency at the ground station in the absence of a planetary atmosphere. This prediction must involve a precise estimation of the spacecraft trajectory, as well as corrections for propagation effects from Mars to ground station (including relativistic motion between transmitter and receiver, Earth's rotation and propagation through interplanetary plasma and Earth's atmosphere and ionosphere).

Applying Lorentz covariant theory of the propagation of light in the (weak) grav-

itational fields of N-body systems, the prediction of the received frequency at the ground station at reception time t_R is given by (Kopeikin & Schäfer 1999)

$$f_R = f_T \frac{1 - \mathbf{k}_R \cdot \mathbf{v}_R/c}{1 - \mathbf{k}_T \cdot \mathbf{v}_T/c} R(\mathbf{v}_R, \mathbf{v}_T, t_R, t_T), \tag{3.2}$$

where the velocities $\mathbf{v}$ must be taken in the barycentric frame at reception and transmission time, and the unit vectors $\mathbf{k}$ point in the direction of wave propagation at those times. Then f_T is the transmission frequency at transmission time, and R is the relativistic factor

$$R(\mathbf{v}_R, \mathbf{v}_T, t_R, t_T) = \left[\frac{1 - (\mathbf{v}_T/c)^2}{1 - (\mathbf{v}_R/c)^2}\right]^{1/2} \left[\frac{a(t_T)}{a(t_R)}\right]^{1/2} \frac{b(t_R)}{b(t_T)} \tag{3.3}$$

with $a(t)$ and $b(t)$ defined in Section 2.2 of Bocanegra-Bahamón et al. (2018). The first bracket represents the special relativistic Doppler shift, the second is a general relativistic correction for proper time, and the third accounts for the light travel delays.

Consulting Figure 3.1, the unit vectors $\mathbf{k}$ from equation 3.2 may be expressed using the ray path angles $\delta_{s,r}$ and $\beta_{e,r}$ in the occultation coordinate system. For the free-space case, i.e. the predicted ray propagation model in the absence of atmospheric refraction, the ray is a straight line, implying $\mathbf{k}_R = \mathbf{k}_T$ and $\delta_r = \beta_r = 0$. In the refractive case, the unit vectors align with the ray path asymptotes plotted in blue. We write:

$$-\mathbf{k}_{R,free-space} = \hat{\mathbf{r}} \sin\delta_s + \hat{\mathbf{z}} \cos\delta_s \tag{3.4}$$

$$-\mathbf{k}_{T,free-space} = \hat{\mathbf{r}} \cos\beta_e + \hat{\mathbf{z}} \sin\beta_e \tag{3.5}$$

$$-\mathbf{k}_{R,detected} = \hat{\mathbf{r}} \sin(\delta_s - \delta_r) + \hat{\mathbf{z}} \cos(\delta_s - \delta_r) \tag{3.6}$$

$$-\mathbf{k}_{T,detected} = \hat{\mathbf{r}} \cos(\beta_e - \beta_r) + \hat{\mathbf{z}} \sin(\beta_e - \beta_r) \tag{3.7}$$

If we now denote $f_R^{free-space}$ as the modelled signal we would receive in the absence of the planet's atmosphere, and $f_R^{detected}$ as the real detected signal, the Doppler residuals are defined as

$$\Delta f = f_R^{detected} - f_R^{free-space}. \tag{3.8}$$

By plugging the expressions for the unit vectors from Equations 3.4-3.7 into Equation

3.2, we obtain an expression for the frequency residuals in terms of the ray path angles:

$$\Delta f = R f_T \left(\frac{c + v_{r,R} \sin(\delta_s - \delta_r) + v_{z,R} \cos(\delta_s - \delta_r)}{c + v_{r,T} \cos(\beta_e - \beta_r) + v_{z,T} \sin(\beta_e - \beta_r)} - \frac{c + v_{r,R} \sin \delta_s + v_{z,R} \cos \delta_s}{c + v_{r,T} \cos \beta_e + v_{z,T} \sin \beta_e} \right)$$

where the subscripts R and T denote reception and transmission time, and subscripts z and r denote velocity components in those respective directions. The angles which appear in the equation satisfy the following conditions:

$$\beta_e + \delta_s = \pi/2,$$
$$\beta_r + \delta_r = \alpha,$$

where α is the so-called bending angle. In order to calculate the bending angle from the residuals in Equation 3.9, one more equation is needed. For this purpose we use the impact parameter a from Figure 3.1:

$$a = |z_R| \sin(\delta_s - \delta_r) = (r_T^2 + z_T^2)^{1/2} \sin(\beta_e - \gamma - \beta_r) \tag{3.9}$$

Hence, for every sampled time step we numerically solve the system of equations 3.9 and 3.9 and obtain the bending angle α and impact parameter a as functions of time.

Now we wish to relate these ray path parameters to atmospheric properties so that we may extract the density, pressure and temperature for each layer of the atmosphere.

Firstly, for the k-th concentric layer of a spherically symmetric atmosphere, the bending angle α as a function of refractive index $n(r)$ can be expressed using the Abel transform (see Born & Wolf (1999) and Fjeldbo et al. (1971)):

$$\alpha(a_k) = -2a_k \int_{r=r_k}^{r=\infty} \frac{d \ln(n(r))}{dr} \frac{dr}{\sqrt{(n(r)r)^2 - a_k^2}} \tag{3.10}$$

Inverting this Abel transform and integrating over all the layers the ray has crossed

gives us the refractive index for the k-th layer:

$$n_k(a_k) = \exp\left\{ \frac{1}{\pi} \int_{a_1}^{a_0} \frac{\tilde{\alpha}_1 da}{\sqrt{a^2 - a_k^2}} + ... + \frac{1}{\pi} \int_{a_k}^{a_{k-1}} \frac{\tilde{\alpha}_k da}{\sqrt{a^2 - a_k^2}} \right\} \tag{3.11}$$

where the $\tilde{\alpha}_i$ is an arithmetic mean of the bending angles α_i, α_{i-1} in a layer.

Having the refractive index n_k enables us to express the total atmospheric refractivity μ_k as

$$\mu_k = (n_k - 1) \times 10^6 = \mu_{n,k} + \mu_{e,k} = \kappa N_n - \frac{N_e e^2}{8\pi^2 m_e \epsilon_0 f^2}, \tag{3.12}$$

where where κ is the mean refractive volume, N_n is the neutral number density, e is the elementary charge, m_e is the electron mass, ϵ_0 is the permittivity of free-space, f is the radio link frequency and N_e is the electron density. The total refractivity is a sum of contributions from the neutral atmosphere (μ_n - dominates at lower altitudes, higher neutral densities) and the ionosphere (μ_e - dominates at higher altitudes, higher electron densities). Assuming the ionospheric contribution to be negligible at the depths we are interested in probing, we directly obtain the neutral number density as a function of height: the vertical density profile $N_n(h)$.

Then we turn to the ideal gas law for the vertical pressure profile,

$$p(h) = kN_n(h)T(h), \tag{3.13}$$

where k is the Boltzmann constant and $T(h)$ is the vertical temperature profile. Assuming hydrostatic equilibrium, this equation may be rewritten for the temperature:

$$T(h) = T(h_0)\frac{N(h_0)}{N(h)} + \frac{\bar{m}}{kN(h)} \int_{h}^{h_0} g(h)N(h)dh \tag{3.14}$$

where $\bar{m}$ is the mean molecular mass, $g(h)$ is the gravitational acceleration and h_0 is the altitude taken to be the top of the atmosphere, yielding the temperature profile for a given boundary condition, the temperature $T(h_0)$. We now have a complete physical solutions for the number density, pressure and temperature profiles of the atmosphere for an observed spacecraft occultation, requiring as input the frequency residuals from Equation 3.9. What follows is a description of the software packages

utilized to compute the residuals from the raw VLBI observation data.

3.3 PRIDE data processing pipeline

Following the observation planning and scheduling as described in the previous chapter, each of the participating ground stations delivers their raw data to JIVE on physical disks in the Mark-5 (MkV)[8] format. The MkV 8-packs of hard drives are the current VLBI standard capable of storing data at high rates up to 2 Gb/s. The data are stored in the time domain, hence the first step in data processing will be to convert to the frequency domain.

1. **Spectrometer** - A software tool that performs a Fast Fourier Transform (FFT) and time integration on the raw MkV data and outputs the power spectrum with a chosen frequency resolution. The input parameters include number of FFT points, FFT integration time, bandwidth and the frequency channel (subband) where the spacecraft signal is located.

   The spacecraft signal can be recognized by a tall, narrow peak at approximately the known transmission frequency, 8.4 GHz (X-band), representing the *carrier tone*. In the case that the spacecraft is also transmitting telemetry by modulating the carrier wave, data bands will be present as symmetrically distributed peaks around the carrier, corresponding to modulation frequencies. An example of the spectrum centered on the carrier tone for a channel 16 MHz wide is shown in the upper portion of Fig. 3.2.

   During the observation time, the frequency/phase of the carrier tone will drift due to the Doppler shift of the spacecraft motion. The smearing of the frequency spectrum is shown in the lower left of Fig. 3.2, in a zoomed view of the averaged time-integrated spectra for the entire duration of the scan (530 sec.) This enables us a first-order estimate of the temporal evolution of the carrier signal (lower right in the same Figure). A sixth-order polynomial is fitted to the initial frequency detections in preparation for the following step.

2. **Tone Tracking** - The spacecraft tracker applies the initial polynomial fit using a window-overlapped add (WOLA) discrete Fourier transform-based algorithm

[8] https://www.haystack.mit.edu/tech/vlbi/mark5/

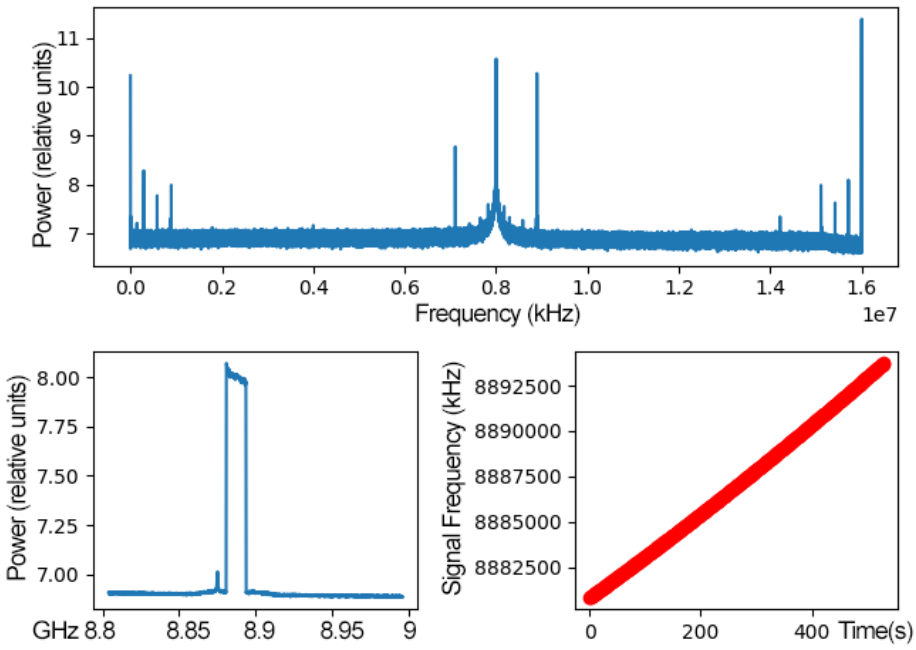

Figure 3.2: Output of the software spectrometer for experiment GR035 with Svetloe station. Top: the last power spectrum read from the scan (total bandwidth, 16 MHz). The narrow peaks at fixed frequencies represent Earth-based radio-frequency interference (RFI). Lower left: Averaged time-integrated spectra for all 530 seconds of the scan, zoomed at the S/C carrier tone. Lower right: Frequency detections of the carrier signal over time.

of the Hilbert transform approximation to extract a narrow band around the spacecraft carrier tone and thus filter out the spacecraft signal into a $\sim$2 kHz band, as opposed to the initial 16 MHz bandwidth. Information about the spacecraft in the complex time domain is expressed with respect to the ground station's local hydrogen maser clock.

3. **Digital Phase-Locked Loop** - The PLL runs high-precision reiterations of the time-integration of overlapped spectra, polynomial fitting and phase correction on the complex narrow bandwidth signal. The initial fit is thus refined to achieve mHz accuracy around the carrier line. The number of FFT points is increased to 2000 with 1 second integration time, resulting in the final time-averaged detections of carrier tone frequencies at each ground station. (Note that the base frequency of the channel, 8412 MHz, should be added to the tone frequencies to obtain the total frequency.) An example of the DPLL output is shown in Figure 3.3.

4. **Frequency residuals** - Now that we have obtained the detected carrier fre-

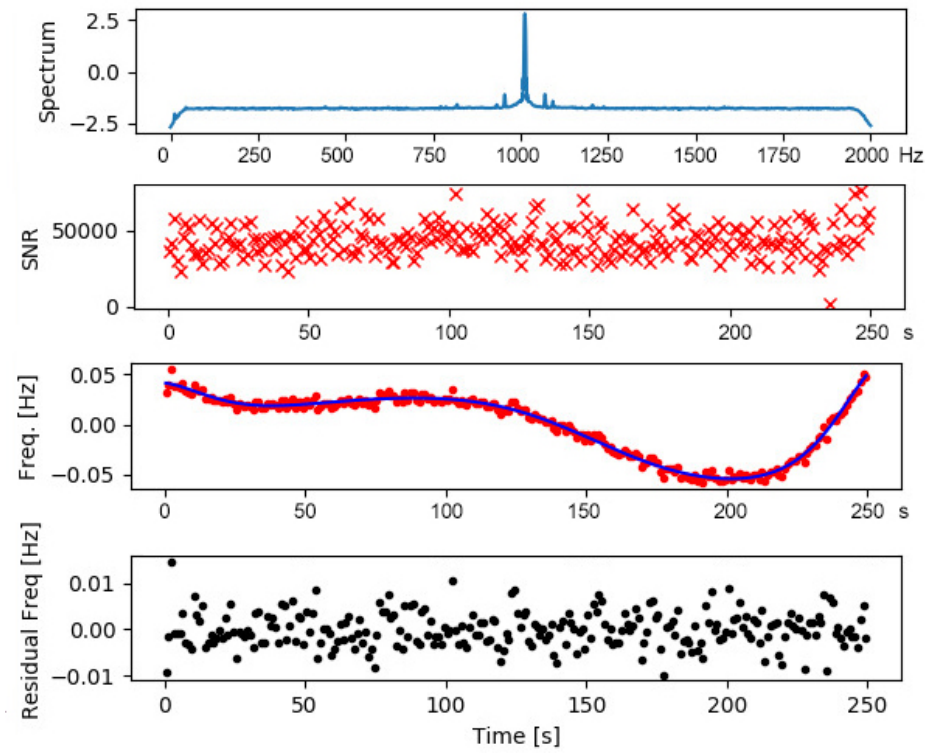

Figure 3.3: Output of the Digital Phase-Locked Loop for experiment GR035 with North Liberty station. From top to bottom: power spectrum of signal in narrow 2kHz band, signal-to-noise ratio, carrier frequency with polynomial fit, residuals of polynomial fit.

quencies, in order to find the frequency residuals $\Delta f = f_R^{detected} - f_R^{free-space}$, it is necessary to compute the prediction $f_R^{free-space}$ for each telescope using Equation 3.2. For this purpose, the precise positions of MEX and all the stations with respect to the Solar System barycenter are required as input for light-travel time corrections. The position of the spacecraft was modeled according to the MEX navigation post-fit orbit provided by the European Space Operations Centre (ESOC). For a detailed explanation of all the relativistic corrections to the signal propagation, see (Bocanegra-Bahamón et al. 2018). An example of the calculated residuals is shown in Figure 3.4.

The effects of the atmosphere and ionosphere are already apparent. The first positive peak around 26610 s corresponds to the main layer of the ionosphere, and the smaller peak that follows it is caused by the second layer. Once immersion into the neutral atmosphere begins, the residuals abruptly drop. Loss of signal is observed after ∼7 Hz, and in the case of Yebes at ∼12 Hz.

5. **Atmospheric profiles module** - The final module uses the MEX navigation

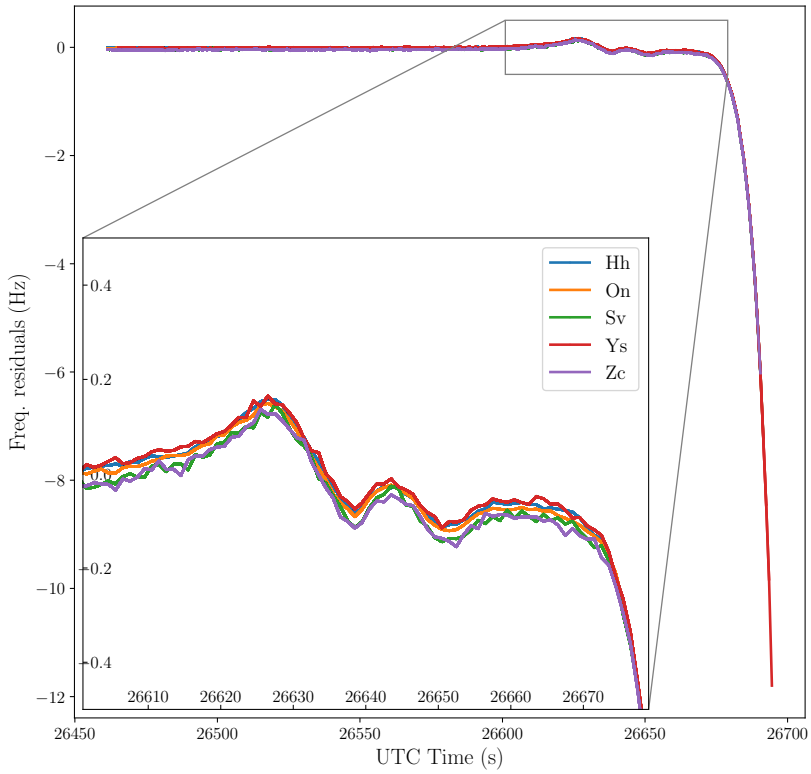

Figure 3.4: Doppler frequency residuals for MEX observed by Haartebeesthoek, Onsala, Svetloe, Yebes and Zelenchukskaya during the occultation of 29th December 2013. Vertical offsets between the residuals for different stations are removed in the baseline correction process.

orbit to define the occultation coordinate system from Figure 3.1 and find the bending angle and impact parameter at each time step using the frequency residuals. The atmosphere is modeled as K concentric spherical layers, the number of which is determined by the integration time step used in the DPLL. This is followed by the Abelian integral inversion to obtain the refractive index (Eq. 3.11), temperature (Eq. 3.14) and pressure (Eq. 3.13).

3.4 Derived atmospheric profiles

The resultant atmospheric ingress profiles are shown in Figure 3.5. In order to solve Eq.3.14, the upper boundary temperature is assumed to be 110 K at 3441 km and the composition of Mars' atmosphere is assumed to be 95.7% CO_2, 2.7% N_2, 1.6% Ar with a mean molecular mass of 0.043503168 kg/mol. The local solar time (LST) at the occultation point is 04:55, corresponding to the position of the Sun in the sky (in other words, the time that would be read on a sundial). The processed stations include Haartebeesthoek, Onsala, Svetloe, Yebes and Zelenchukskaya, of

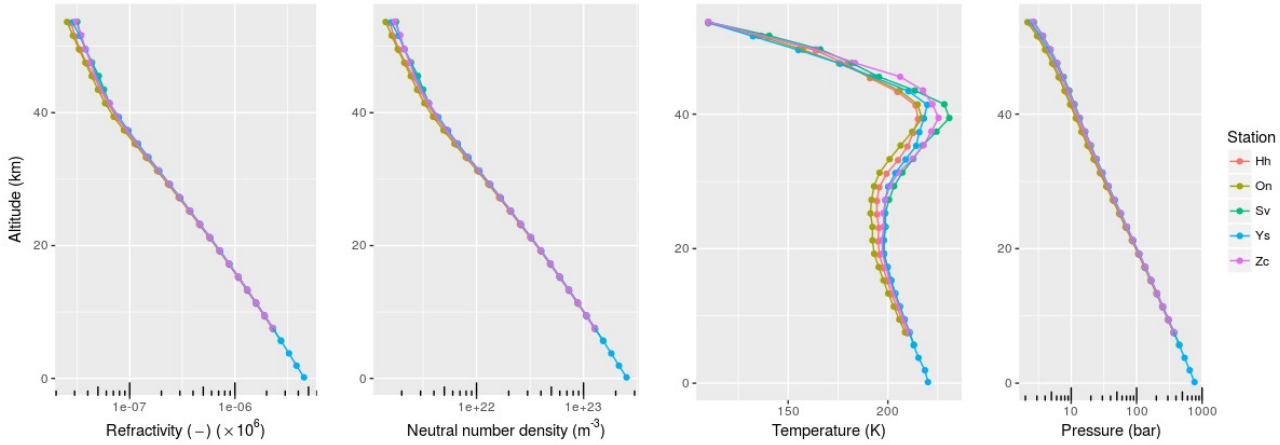

Figure 3.5: Vertical profiles of refractivity, neutral number density, temperature and pressure derived from the MEX radio occultation data. Stations included are Haartebeesthoek, Onsala, Svetloe, Yebes and Zelenchukskaya.

which Yebes has managed to acquire the lowest altitude measurements (with respect to an ellipsoid defined using Mars' radius and flattening value) nearly down to the surface. At approximately 40 kilometers altitude, a temperature shift from the cold mesosphere to the warm troposphere is observed. An overview of the lowest altitude parameters for each of the stations is shown in Table 3.2.

Table 3.2: **Lowest altitude atmospheric parameters per observing station**

Station	Alt. (km)	Lat.(^{o})	Long. (^{o})	$\mu(\times 10^6)$	$n_n(\times 10^{23}\mathrm{m}^{-3})$	T (K)	p (bar)
Hh	7.412	-174.5196	62.4978	2.303	1.283	209.825	371.654
On	7.561	-174.6032	62.4441	2.279	1.270	208.594	365.668
Sv	5.714	-174.6566	62.3893	2.733	1.523	213.072	447.905
Ys	0.162	-174.5316	62.4428	4.531	2.525	220.075	767.062
Zc	7.602	-174.5460	62.4848	2.281	1.271	210.523	369.449

In conclusion, the PRIDE open-loop signal processing method has enabled the reconstruction of high-resolution vertical atmospheric profiles for a column of the Martian atmosphere down to less than 10 kilometers from the surface.

4 New frontiers for PRIDE

In this section, we discuss novel ideas for PRIDE applications to planetary science, such as bistatic radar or the LaRa (Lander Radioscience) experiment on Mars.

4.1 Bistatic radar

Bistatic radar is a method of remote probing by 'bouncing' a radio signal off a planetary surface, capable of providing terrain information on the scale from ten to about 250 wavelengths which corresponds to structures ranging from centimeters to hundreds of meters. Surface properties at these scales are important for landers and rovers as well as studies of geophysical evolution. PRIDE could assist in choosing optimal landing and roving sites and areas of geological interest, as signal reflection depends on dielectric properties of the soil. A diagram of the downlink bistatic radar configuration for spacecraft is shown in Figure 4.1.

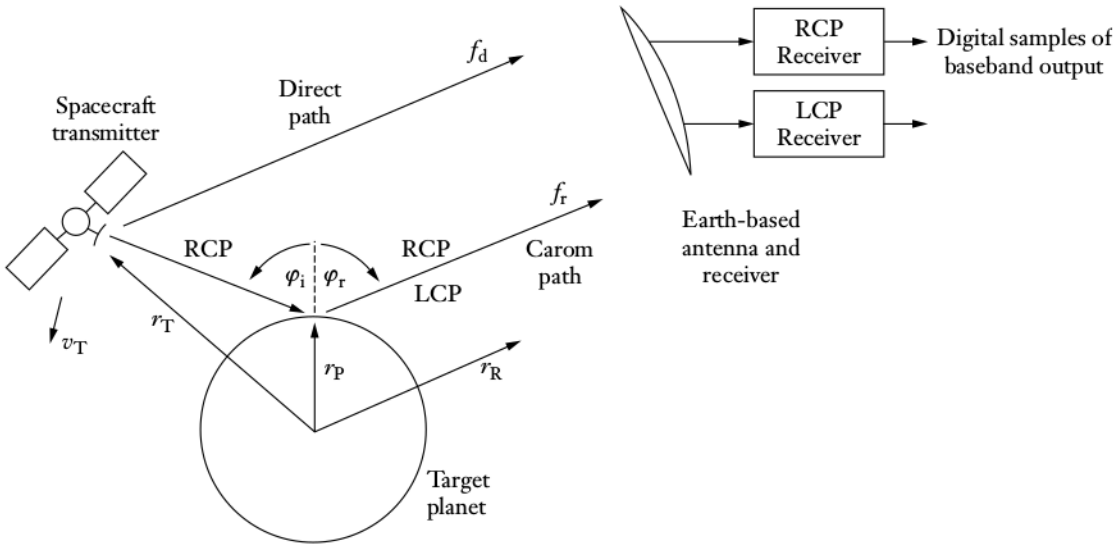

Figure 4.1: Downlink bistatic radar geometry. Subscripts denote T for transmitter, P for (specular) reflection point, R for receiver. Rate of change of the carom path length introduces a Doppler shift f_r which differs from the Doppler shift along the direct path f_d. (Source: Willis et al. (2007))

Whereas classic (monostatic) radar involves a radio wave transmitter and receiver in the same location, in the bistatic case the transmitter and receiver are separate. In a downlink experiment a spacecraft bounces a radio wave off the surface of the planet to be detected by an antenna on Earth, whereas in an uplink experiment an antenna on Earth transmits a pulse to the target body and the spacecraft re-

ceives the signal echo. Downlink experiments have been previously performed on the Moon, Venus, Mars and Titan (see Willis et al. (2007) for a historical overview of the method). Uplink experiments in theory offer better detectability because of the higher transmitting power of a ground antenna ($\sim$1 MW, as opposed to $\sim$100 W for a spacecraft antenna), but they require specialized receiver hardware to be installed on the spacecraft[9] as well as modified attitude control for the craft during the experiment (pointing the antenna towards the planet), therefore straining the mission time scheduling and budget. This is where utilizing the EVN antennas at PRIDE's disposal would prove useful: the greater number of ground stations with larger diameters and higher sensitivities would enable downlink experiments to be feasible even for distant outer Solar System bodies, using nothing but the standard radio transmitting equipment found on orbiting spacecraft.

The experiment is performed as follows: the spacecraft transmits an unmodulated carrier signal towards the planetary surface, which is then reflected at the specular point and the scattered radiation travels along the carom path to the receiver on Earth. Due to the varying rates of change of the direct and reflected paths, the receiver is able to distinguish the carrier signal coming directly from the spacecraft from its echo. Assuming that the surface reflects *quasi-specularly*, i.e. the incident and reflected wave vectors are in the same plane and $\varphi_i = \varphi_r = \varphi$, classical Fresnel optics apply (Fjeldbo 1964; Simpson 1993). The infinitesimal echo power received from a surface element dS can be expressed using the radar equation:

$$dP_R = \frac{P_T G_T}{4\pi|\mathbf{r}_P - \mathbf{r}_T|^2}\sigma\frac{A_R}{4\pi|\mathbf{r}_R - \mathbf{r}_P|^2}, \tag{4.1}$$

where the first term contains the S/C antenna properties; the transmitting power P_T and the directional antenna gain G_T, and the third term contains the receiver properties; the effective collecting area of the antenna aperture A_R. The monostatic radar is then a special case when $\mathbf{r}_P - \mathbf{r}_T = \mathbf{r}_R - \mathbf{r}_P$ and the bistatic angle is zero. The σ in the equation denotes the specific bistatic radar cross-section which, for a uniformly illuminated perfectly conducting planetary surface with Gaussian roughness

[9]The first such dedicated uplink hardware has been launched with the New Horizons spacecraft which has successfully performed the longest distance uplink bistatic radar experiment during its fly-by of Pluto in 2015, when the planet was 33 AU away from Earth (Linscott et al. 2016). It will attempt to push this record further when it reaches 2014 MU_{69} in the Kuiper Belt in January 2019.

statistics, is given by (Fjeldbo 1964):

$$\sigma = \frac{64\pi^3 P_R |\mathbf{r}_R|^2 |\mathbf{r}_T|^2}{P_T G_T G_R \lambda^2}. \tag{4.2}$$

Now, if the angles $\varphi_i = \varphi_r > 0$, we speak of *forward specular reflection*, and in the case of $\varphi_i = \varphi_r = 0$, of *specular backscatter*, when most of the radiation is scattered in the direction of the transmitter. A general cross-section is a sum of these different regimes, but observation has shown that the quasi-specular component is negligible in the case of icy Galileian satellites and the backscatter lobe dominates. For such a target, the cross-section would be

$$\sigma = \pi \left(\theta_T |\mathbf{r}_P - \mathbf{r}_T|\right)^2 \eta(\varphi), \tag{4.3}$$

where θ_T is the spacecraft antenna HPHW (half-power half-width) and $\eta(\varphi)$ is the power reflectivity (ratio of observed signal strength to the signal expected from a perfectly conducting sphere) which is equal to the square of the Fresnel voltage reflection coefficients. The dependence of these coefficients on the dielectric constant of the surface materials is known from geometric optics, hence dielectric properties of the soil can be obtained from the measured reflectivity. Furthermore, the dielectric constant can be related to density of the soil using known methods (such as the Rayleigh mixing formula), offering further geological insight.

Introducing Eqn.4.3 into 4.2 with $\mathbf{r}_R \approx |\mathbf{r}_R - \mathbf{r}_P|$ and $\mathbf{r}_T \approx |\mathbf{r}_P - \mathbf{r}_T|$ yields

$$P_R = \frac{P_T G_T G_R}{4} \left(\frac{\lambda \theta_T}{4\pi |\mathbf{r}_R - \mathbf{r}_P|}\right)^2 \eta(\varphi) \tag{4.4}$$

for the total power at the receiver. It is important to note that in reality, due to the antenna beamwidth, this power will be distributed into a set of *glints* arising from reflections on a small scattering region centered around r_P (Figure 4.2). As the rays from each of these scattering points have slightly different path lengths and Doppler shifts, the resulting echo signal will be broadened into a bell-like curve. The closer the surface is to a reflecting sphere, the smaller the spread, and likewise, the rougher the surface or the more rapidly the spacecraft moves, the larger the spread. The corresponding half-width of the echo spectrum for a special case in which the spacecraft velocity $\mathbf{v}$ is in the same plane as the incident and reflected wave was

approximated in Simpson (1993) and is equal to

$$B_{obs} = \frac{4|\mathbf{v}|}{\lambda} \sin\alpha \sin\theta_T, \tag{4.5}$$

where α is the angle between the antenna pointing and the spacecraft velocity.

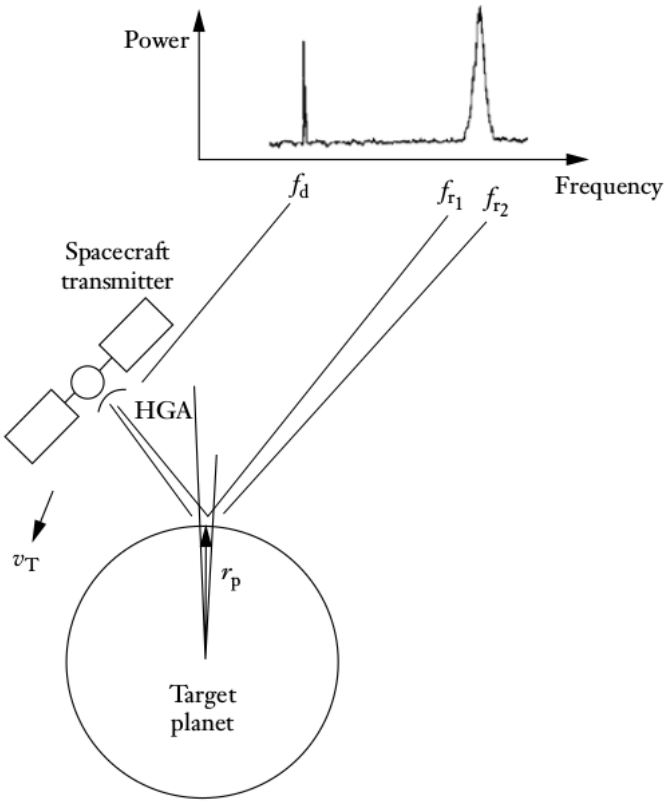

Figure 4.2: Formation of the spacecraft signal echo on a real planetary surface. Each point on the surface within the illumination pattern of the high-gain antenna (HGA) contributes to the echo with a slightly different Doppler shift, dispersing the signal into a bell-like curve. (Source: Willis et al. (2007))

A useful measure of our ability to measure the properties of the signal is the detectability D, defined as

$$D = \frac{P_R}{P_N}\sqrt{B_{obs}}, \tag{4.6}$$

where $P_N = kT_{sys}\Delta f$ is the noise power in the receiver due to the system noise temperature T_{sys}, multiplied by the Boltzmann constant and the bandwidth of interest (in our case the echo bandwidth B_{obs}). Using Equations 4.4 and 4.5, we can rewrite the detectability as

$$D = \frac{P_T G_T G_R}{128\pi^2 k T_{sys} |\mathbf{r}_R - \mathbf{r}_P|^2} \left(\frac{\theta_T^3 \lambda^5}{|\mathbf{v}| \sin\alpha}\right)^{1/2} \eta(\varphi). \tag{4.7}$$

Now we are equipped to test the detectability for a potential future bistatic radar experiment with PRIDE. A valuable opportunity would be ESA's JUpiter ICy moons Explorer (JUICE, Fig.4.3) which is scheduled to perform multiple close fly-bys of the Galileian moons during nominal mission operation time in 2029-2032. Our test example will be a Europa flyby on October 5th 2030, denoted '6E1' according to the Consolidated Report on Mission Analysis (CReMA) version 3.2.[10] The flyby will occur on the dayside with velocity ∼3.8 km/s and closest approach distance of ∼400 km. The surface point directly below the closest approach is set as the specular point and the Effelsberg 100-m dish is selected as the receiver. Converged Newtonian light travel time corrections are applied to the state vectors generated by the ESA WebGeoCalc[11] interface.

Figure 4.3: JUICE mission insignia. (Copyright: ESA)

The relevant plots are shown in Figure 4.4 for transmitter[12] and receiver parameters from Table 4.1. The reflectivity was assumed to be $\eta(\varphi) \approx 1$, which was demonstrated by experiment to be a sufficient first order approximation for icy Gallileian satellites. The moment of nearest flyby around 145 minutes into the observation is evident from the transmitter distance in the upper left plot, corresponding to zero incident angle in the upper right plot. The two lower plots depict the Doppler spreading of the signal and its detectability. Because of the very high velocity and low altitude of the spacecraft during flyby, the signal will be broadened up to 7 kHz. However, owing to Effelsberg's high G_R/T_{sys} ratio in Equation 4.7, the signal detectability does not dip below 30 dB. For comparison, this ratio is 4 times lower for a 70-meter NASA DSN tracking station. The detectability increases further as the spacecraft spends

[10] SPICE kernels for JUICE: https://www.cosmos.esa.int/web/juice/products-crema-3.2
[11] http://spice.esac.esa.int/webgeocalc/
[12] Parameters were obtained from the JUICE Yellow Book and are subject to change during mission development.

long amounts of time at incidence angles near 60^o, which were shown to be optimal for dielectric constant measurements of the soil. Overall, the performance of EVN antennas shows potential for performing a successful bistatic radar experiment with JUICE.

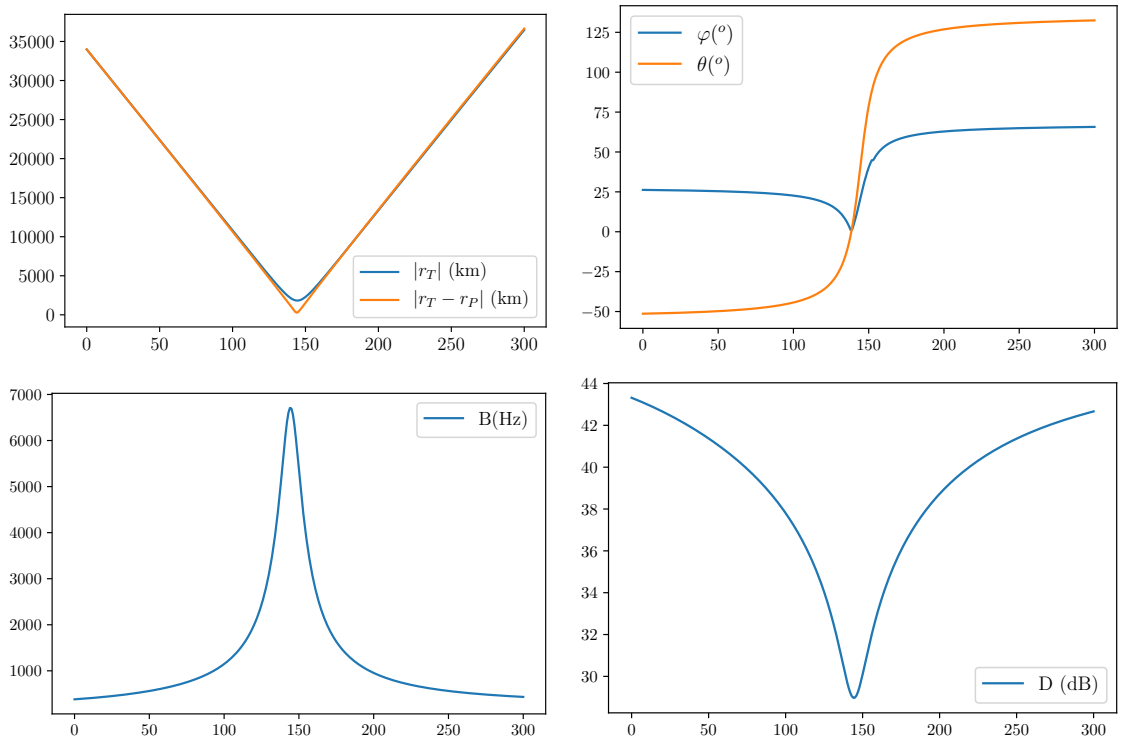

Figure 4.4: Plots of transmitter distance to specular point and planet center, relevant angles, bandwidth and detectability for a potential bistatic radar experiment with Effelsberg as part of JUICE Europa flyby 6E1. φ denotes incident angle and θ denotes the angle between $\mathbf{r}_T$ and $\mathbf{r}_R$. The x-axis is time in minutes.

Table 4.1: **Radio parameters for bistatic radar**

	JUICE	Effelsberg
Antenna (m)	2.54	100
HPHB (^{o})	0.8	0.02
Trans. Power P_T(W)	100	–
Gain (dBi)	50	181.5
T_{sys} (K)	–	21

4.2 Mars Lander Radioscience (LaRa)

Yet another opportunity to deploy PRIDE is presented with the LaRa instrument (Dehant et al. 2009) which will be launched aboard the ESA & Roscosmos ExoMars 2020 mission. The mission will consist of a rover and a surface platform, the latter of which will host the shoebox-sized LaRa module at a fixed point on the surface

of Mars. LaRa will contain an X-band transponder which will exchange a two-way Doppler signal via radio link with Earth-based tracking stations over the span of at least one Martian year. The amount of science output depends on the availability of observing antennas, where PRIDE could readily reinforce the DSN and Estrack in shadow-tracking mode.

An outline of the LaRa experiment is shown in Figure 4.5. Coherency of the X-band radio link signal is ensured by the high-precision maser clocks at the receiving stations, whose locations are known to centimeter precision thanks to VLBI measurements, in order to obtain the desired 0.1mm/s Doppler precision for scientific use. This would enable us to pinpoint LaRa's position on the Martian surface down to several tens of centimeters at the distance of about 200 million kilometers. As LaRa rotates with the planet, the Doppler shift of its signal would provide an unprecedented measure of the variation of Mars' rotation speed and the orientation of its rotation axis in space (precession and nutation) as well as polar motion and the seasonal redistribution of mass between the atmosphere and the polar caps. The primary objective of LaRa is to constrain the precession with a factor of 4 compared to present-day measurements, which would then enable geological modelling of the Martian interior composition as precession is inversely proportional to the polar principal moment of inertia. Just as a boiled egg rotates differently than a raw one, measurements of the moments of inertia of Mars would answer the question on whether the Martian core is solid or liquid and yield a remote sensing of sorts into its dimensions down to several tens of kilometers.

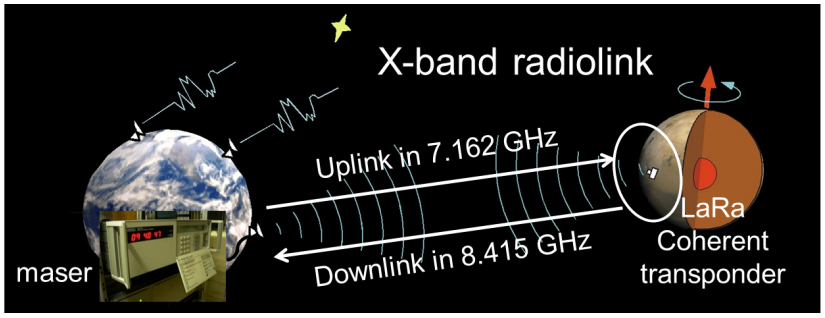

Figure 4.5: Sketch of the LaRa experiment setup. (Source: https://lara.oma.be/)

As PRIDE has routinely demonstrated the ability to deliver high-precision Doppler observables from orbiters at Mars, its natural extension to landers will prove a valuable reinforcement to the LaRa experiment.

5 Summary and outlook

5.1 Summary

The Planetary Radio Interferometry and Doppler Experiment (PRIDE) utilizes methods and instrumentation of Very Long Baseline Interferometry (VLBI) to offer a valuable enhancement to radio science returns from planetary missions. Using a network of radio telescopes across the globe, PRIDE is able to offer unprecedented precision in determining the state vectors of spacecraft in the Solar System, which can be applied to a variety of studies from gravimetry and atmospheric science to investigations of coronal mass ejections.

The scheduling of a PRIDE experiment was discussed in Section 2 of this Thesis on the example of a dual-spacecraft observation involving two orbiters at Mars. A finding chart was generated for Mars with respect to extragalactic radio sources from the Radio Fundamental Catalog, isolating the sources located at less than 2 arcminutes from Mars' ephemeris for the purpose of in-beam phase-referencing. The visibilities of these sources were then tested for European VLBI Network (EVN) and Very Long Baseline Array (VLBA) telescopes at the target dates, yielding five observing opportunities which will form the basis of a long-term observing campaign throughout 2018/2019 for planetary studies of the Martian system, as well as sharpening of the PRIDE technique.

The data from an example PRIDE experiment was reduced in Section 3 and applied to a radio occultation study of the Martian atmosphere. A radio occultation experiment is based on measuring the properties of a spacecraft signal as it travels through a planet's atmosphere during ingress or egress behind the planetary horizon. The variation of the signal frequency with respect to a predicted model was shown to correspond to a vertical variation of refractivity within the column of atmosphere above the occultation point. The obtained refractivity profile enabled us to find the vertical density, pressure and temperature profiles with some simple assumptions about the properties of the Martian atmosphere. Data from five stations was processed in the experiment and yielded profiles down to less than 10 kilometers from the surface.

5.2 Outlook

PRIDE has been demonstrating its versatility and precision since the initial experiments over a decade ago. Due to previous achievements, PRIDE has been selected by ESA to provide high-precision tracking for the JUpiter ICy moons Explorer mission (JUICE) launching in 2022. One of the ways in which PRIDE could support this mission was discussed in Section 4, involving a bistatic radar experiment which would infer the dielectric properties of the surface of Europa by studying a radar signal reflected from its surface. Such an experiment was demonstrated to be feasible with the EVN telescopes, offering solid detectability throughout the event. Furthermore, a valuable opportunity for PRIDE was investigated in terms of the LaRa experiment, in which PRIDE would track the signal transmitted from a lander planted on the Martian surface as part of ESA's ExoMars 2020 mission. The return from this experiment would yield geological insight into the internal structure of Mars.

Overall, the numerous applications of PRIDE which come at no additional financial or scheduling cost to space missions ensure that it will remain a powerful tool for planetary radio science in the decades to come.

6 Prošireni sažetak

6.1 Uvod

Preciznost je oduvijek bila odlučujući čimbenik u (ne)uspjesima svemirskih misija. U interesu smanjivanja margine pogreške pri praćenju svemirskih letjelica, svemirski znanstvenici i tehnolozi posegnuli su za interdisciplinarnim savezništvom s radio astronomijom, osobito dugobazičnom interferometrijom (*Very Long Baseline Interferometry* - VLBI). Dugobazična interferometrija uključuje mrežu radioteleskopa koji mogu biti rasprostranjeni po svim kontinentima, a čak i u Svemiru na radioteleskopskim satelitima koji istovremeno promatraju istu metu. Iako teleskopi nisu fizički povezani, podaci se na njima snimaju uz ultraprecizne vremenske oznake s maserskih satova, što kasnije omogućuje njihovu *korelaciju* u centralnoj ustanovi za obradu podataka, uključujući dobivanje interferometrijske slike iz signala zabilježenih na svakom teleskopu postupkom *sinteze* (za matematički i povijesni opis VLBI metode vidi Ryle (1961) i Thompson et al. (2017)). Najveće VLBI mreže čine European VLBI Network (Slika 1.2) i Very Long Baseline Array (Slika 1.3) koje su u mogućnosti postići miliarksekundnu rezoluciju.

Uz određene aproksimacije (Duev et al. 2012), VLBI metode mogu se primijeniti na praćenje signala s radiotransmitera svemirskih letjelica. Inicijativa PRIDE: Planetarni Radio Interferometrijski i Doppler Eksperiment pokrenuta je na vodećem europskom institutu za VLBI, Joint Institute for VLBI ERIC (JIVE). Dok tradicionalne metode praćenja letjelica u dubokom svemiru koriste NASA-in Deep Space Network ili ESA-in Estrack, PRIDE koristi svjetske VLBI mreže, uključujući EVN i VLBA uz dodatna pojačanja australskih, korejskih i japanskih teleskopa. Prednost PRIDE-a nad uvriježenim praćenjem pomoću "zatvorene petlje" (Kinman 1992) jest veća preciznost i stabilnost u određivanju pozicije i brzine letjelice na skalama od 50 m i 30 μm/s u Marsovoj orbiti (Bocanegra-Bahamón et al. 2018; Duev et al. 2016) što pritom ne zahtijeva dodatan vremenski ili financijski trošak pri planiranju misija. Međutim, PRIDE metoda nije u mogućnosti dati vektor stanja letjelice u živom vremenu, nego se njena putanja mora rekonstruirati u naknadnoj obradi signala snimljenog s teleskopa. PRIDE također zahtijeva da se u kutnoj blizini letjelice na nebu nalazi tzv. *fazni kalibrator*, nerazlučeni izvor radio zračenja poznatih svojstava koji se koristi kao referenca da bi se signal mogao pročistiti od atmosferskih i instrumen-

talnih pogrešaka. Zbog toga, planiranje PRIDE opservacije uključuje razmatranja mnogo faktora, od transmisijskog vremena letjelice do njene vidljivosti za pojedini teleskop i dostupnosti faznog kalibratora. Tijek planiranja za jednu PRIDE opservaciju iznešen je u Poglavlju 2.

6.2 Planiranje PRIDE opservacije

Od šest trenutno aktivnih orbitera oko Marsa, dva trenutno pripadaju Europskoj Svemirskoj Agenciji (ESA): *Mars Express* (MEX) i *ExoMars Trace Gas Orbiter* (TGO). Obje letjelice emitiraju signal of 8.6 GHz prema Zemlji te bi se promatranjem Marsa uz dovoljno veliku frekventnu širinu (*bandwidth*) moglo detektirati oba signala i rekonstruirati vektore stanja za obje letjelice istovremeno. Takav dvostruki PRIDE eksperiment nije prethodno izveden te bi se, osim za pooštravanje PRIDE tehnike, izvedene putanje letjelica mogle koristiti za ultrapreciznu gravimetriju i izračun Marsove efemeride.

Prvi je korak generirati mapu Marsovih nebeskih koordinata u periodu od interesa (2 godine) te pronaći prilike kada Mars mimoilazi potencijalne fazne kalibratore. U tu svrhu, koristimo se efemeridama Jet Propulsion Laboratoryja DE432s (Folkner et al. 2014) koje sadržavaju najmoderniji model Sunčevog sustava za namjenu navigacije svemirskih letjelica. Nakon izračuna Marsovih koordinata u traženom periodu, pretražujemo Radio Fundamental Catalogue (RFC) (Petrov 2017), trenutno najpotpuniji katalog kompaktnih radioizvora nastao analizom svih VLBI programa od 1980. godine te izoliramo 278 izvora koji se nalaze unutar 2 stupnja od Marsove putanje (Slika 2.2). Ovi izvori mogli bi se koristiti kao fazni kalibratori uz uvjet da se teleskopi periodički pomiču između mete i kalibratora svakih desetak minuta (tzv. ”kimanje”, *nodding*). Maksimalna preciznost mogla bi se ostvariti dodatnim postroženjem kriterija na dvije lučne minute, u kojem slučaju bi se i letjelice i kalibrator nalazili unutar zrake (*beam*) svih teleskopa. Taj uvjet sužava broj prilika na pet navedenih u Tablici 2.1.

Od navedenih pet, samo prva prilika 14. lipnja 2018. između 04:00 i 15:00 po univerzalnom vremenu (UTC) s kalibratorom J2036-2146 poklapa se s vremenskim periodom aktivnosti EVN-a koja je raspisana u natječaju. Kako bismo zatražili točno promatračko vrijeme, nužno je provjeriti za koje od EVN-ovih teleskopa će Mars biti

vidljiv. Pritom koristimo SCHED, univerzalni program za stvaranje i distribuciju promatračkih rasporeda za VLBI mreže. SCHED može proizvesti grafove kao na Slici 2.4 koji daju informacije o vidljivosti i elevaciji izvora nad horizontom tijekom ciljanog vremenskog perioda. Vremena vidljivosti za pojedine teleskope navedena su u Tablici 2.3. Uzevši u obzir poluširinu zrake teleskopa (HPBW [rad] $= \lambda/D$, gdje je D promjer), preostaje nam pet teleskopa koji bi bili u mogućnosti promatrati izvor i kalibrator istovremeno, a to su Yebes, Medicina, Wettzell, Noto i Hartebeesthoek od 04:00 do 06:00 UTC. Ovako podešen eksperiment imat će očekivanu preciznost of 100 metara u Marsovoj orbiti (vidi Folkner et al. (1993) za analizu pogrešaka).

Ostala četiri promatračka termina mogu se izvršiti pomoću VLBA mreže unutar predviđenog promatračkog termina za 2018./2019. godinu. Uzevši u obzir da jedan od kalibratora nema dovoljno podataka o svojstvima u RFC katalogu, preostaju tri promatračke prilike sa Slike 2.5. Srećom, Mars je u sva tri termina (2.12.2018., 14.1.2019. i 27.9.2019.) vidljiv za sve VLBA postaje te smo u mogućnosti ostvariti vrlo duga promatračka vremena s do 10 teleskopa istovremeno. Raspored je prikazan u Tablici 2.5.

6.3 Primjer PRIDE eksperimenta: Proučavanje Marsove atmosfere

U Poglavlju 3 iznosimo primjer obrade podataka za prethodno izvršenu PRIDE opservaciju Mars Express orbitera iz 29. prosinca 2013. Pritom demonstriramo kako se PRIDE opservable mogu koristiti za planetarnu znanost; konkretno, za radiookultacijski eksperiment.

Radiookultacija signala (Fjeldbo et al. 1971) događa se kada svemirska letjelica ”zalazi” ili ”izlazi” iza planetarnog horizonta pri čemu se svojstva njenog signala mijenjaju zbog propagacije kroz planetarnu atmosferu. Ukoliko je vektor stanja letjelice dovoljno precizno poznat, može se modelirati predviđeni Dopplerov signal u odsustvu atmosferskih efekata te se njegovom usporedbom sa stvarnim signalom mogu izračunati svojstva poput refraktivnosti, brojčane gustoće, tlaka i temperature za stupac atmosfere kroz koji se signal lomi. PRIDE je prethodno demonstrirao izračun atmosferskih parametara za Veneru do većih dubina nego što je moguće s ESA-inim i NASA-inim tradicionalnim mrežama za praćenje (Bocanegra-Bahamón 2018, u pripremi).

Geometrija radiookultacije prikazana je na Slici 3.1. Kako signal letjelice prolazi kroz sve dublje atmosferske slojeve, realni dio indeksa loma mijenja se s visinom te direktno utječe na fazu signala što je mjerljivo kao promjena frekvencije tona nositelja. Uz pretpostavke da je valna duljina signala manja od skale na kojoj se atmosferska svojstva znatno mijenjaju, primjenjivi su zakoni klasične geometrijske optike te je jednadžba zrake u sfernosimetričnom mediju indeksa loma $n(\mathbf{r})$ dana diferencijalnom jednadžbom (Born & Wolf 1999):

$$\frac{\mathrm{d}}{\mathrm{d}s}\left(n\frac{\mathrm{d}\mathbf{r}}{\mathrm{d}s}\right) = \nabla n. \tag{6.1}$$

U našem je interesu invertirati ovu jednadžbu kako bismo iz parametara α (kuta loma) i a (ulaznog parametra) mogli izračunati profil refraktivnosti. Ovi se parametri mogu dobiti razmatranjem geometrije i Dopplerovih reziduuma signala. Ako označimo s f_R^{vakuum} model signala koji je uz relativističke korekcije očekivan na teleskopu u odsustvu planetarne atmosfere (Bocanegra-Bahamón et al. 2018; Kopeikin & Schäfer 1999), a s $f_R^{detektirano}$ stvarni detektirani signal, Dopplerove reziduume definiramo kao

$$\Delta f = f_R^{detektirano} - f_R^{vakuum}. \tag{6.2}$$

Fjeldbo et al. (1971) je pokazao kako se rješavanjem sistema jednadžbi za α, a i Δf dobiva kut loma, a iz njega Abelovim transformatom vertikalni profil indeksa loma

$$n_k(a_k) = \exp\left\{\frac{1}{\pi}\int_{a_1}^{a_0}\frac{\tilde{\alpha}_1 da}{\sqrt{a^2-a_k^2}} + ... + \frac{1}{\pi}\int_{a_k}^{a_{k-1}}\frac{\tilde{\alpha}_k da}{\sqrt{a^2-a_k^2}}\right\} \tag{6.3}$$

gdje su $\tilde{\alpha}_i$ aritmetičke sredine kutova loma između sfernih slojeva i i $i-1$, a s indeksom k označen je najdublji sloj atmosfere u koji signal prodire. Indeks loma daje refraktivnost $\mu_k = (n_k - 1) \times 10^6$ koja je za neutralnu atmosferu direktno proporcionalna s brojevnom gustoćom. Zakon idealnog plina $p(h) = kN_n(h)T(h)$ i pretpostavka hidrostatske ravnoteže daju konačno i temperaturni profil,

$$T(h) = T(h_0)\frac{N(h_0)}{N(h)} + \frac{\bar{m}}{kN(h)}\int_h^{h_0} g(h)N(h)dh, \tag{6.4}$$

gdje je $\bar{m}$ srednja molekularna masa, g je gravitacijska konstanta i h_0 je visina uzeta

kao vrh atmosfere s pretpostavljenim rubnim uvjetom $T(h_0)$.

Obrada podataka zaprimljenih s teleskopa i rješavanje gore navedenih jednadžbi izvodi se u pet PRIDE modula.

- **Spektrometar** - Softverskim alatom prvo se izvodi brzi Fourierov transformat i vremenska integracija podataka kako bi ih se prebacilo u frekventnu domenu. Ujedno se locira signal letjelice, prepoznatljiv kao visok vrh na gornjem dijelu Slike 3.2. Vremenska evolucija signala (donji desni dio iste Slike) aproksimira se polinomom šestog reda.

- **Praćenje tona** - Koristeći polinomne koeficijente, signal letjelice se filtrira sa širokog pojasa od 8 ili 16 MHz na preciznih 2 kHz.

- **Digitalna fazna petlja** - Prethodni koraci se reiteriraju s visokom preciznošću i faznim korekcijama, povećavajući određenost signala do na razinu mHz. (Prikaz na Slici 3.3).

- **Dopplerovi reziduumi** - Služeći se navigacijskom orbitom letjelice koju dostavlja Europski centar za svemirske operacije (ESOC) izračunava se predviđeni Dopplerov signal i oduzima od detektiranog signala. Rezultantni reziduumi za pet postaja prikazani su na Slici 3.4.

- **Atmosferski profili** - Posljednji modul izračunava kut loma i ulazni parametar za svaki vremenski korak te invertira Abelov transformat kako bi dao vertikalne profile refraktivnosti, gustoće, tlaka i temperature.

Rezultantni vertikalni profili za naš radiookultacijski eksperiment s Mars Expressom prikazani su na Slici 3.5, a najdublje vrijednosti atmosferskih parametara koje je svaka od postaja uspjela izmjeriti navedene su u Tablici 3.2. Atmosferska svojstva su uspješno pronađena za visine manje od 10 kilometara od površine, uz posebno uspješnu detekciju na teleskopu Yebes koji je zadržao signal na nekoliko stotina metara od same površine Marsa.

6.4 Nove prilike za PRIDE

Poglavlje 4 posvećeno je diskusiji novih primjena za PRIDE u sklopu bistatičkog radara i geološkog eksperimenta za sletač na Marsu.

Bistatički radar metoda je proučavanja dielektričnih i reljefnih svojstava planetarnih površina "odbijanjem" radio vala od njihovu površinu. Ovakav eksperiment daje povratnu informaciju na skalama od desetaka do oko 250 valnih duljina, što odgovara prostornim dimenzijama od centimetara do stotina metara. Strukture na ovoj skali važne su za sletače i vozila kao i za studije geofizikalne evolucije. Dijagram bistatičke konfiguracije vidljiv je na Slici 4.1.

Bistatički radar razlikuje se od monostatičkog po tome što emiter i detektor radio vala nisu na istom mjestu. Pritom se može raditi o konfiguraciji u kojoj zemaljska antena odašilje radiopuls prema planetu, a letjelica ga prima (*uplink*) ili obratno (*downlink*). Budući da većina letjelica nije opremljena instrumentima koji bi mogli dovoljno precizno analizirati signal, interesira nas konfiguracija u kojoj bi letjelica odaslala puls, a antene EVN-a ga detektirale. Konkretno, analizirat ćemo izvedivost ovakvog eksperimenta za ESA-inu JUpiter Icy moons Explorer (JUICE) misiju tijekom bliskog leta kraj Jupiterovog ledenog mjeseca Europe.

Uz pretpostavku kvazi-spekularne refleksije na površini planeta, u kojoj su ulazni i izlazni val u istoj ravnini, primjenjivi su zakoni klasične Fresnelove optike (Fjeldbo 1964). Aproksimativni analitički izrazi za radarski presjek i detektiranu snagu signala u slučaju ledenih Jupiterovih mjeseca dani su u Simpson (1993) i Willis et al. (2007). Između ostalog, reflektirani signal bit će i raspršen u zvonoliku krivulju kao na slici 4.2 ovisno o grubosti površine, poluširini zrake antene na letjelici i njene brzine. Širina signala utječe na našu sposobnost da ga detektiramo, i to po formuli za detektabilnost

$$D = \frac{P_R}{P_N}\sqrt{B_{obs}}, \tag{6.5}$$

gdje je $P_N = kT_{sys}B_{obs}$ šum na detektoru zbog sistemske temperature T_{sys}, k je Boltzmannova konstanta, a B_{obs} širina signala.

Detektabilnost je izračunata za bliski susret JUICE-a i Europe koji je planiran za 5. listopada 2030. godine uz 100-metarski Effelsberg teleskop kao promatrač te je prikazana na donjem desnom grafu na Slici 4.4 uz parametre iz Tablice 4.1. Letjelica pritom prolijeće na 400 kilometara od površine s brzinom oko 3.8 km/s. Unatoč velikoj brzini i širenju signala do 7 kHz, Effelsberg demonstrira povoljne detektabilnosti iznad 30 dB. U usporedbi, NASA-ina 70-metarska antena pokazala bi četverostruko lošije rezultate, što čini PRIDE obećavajućim alatom za studije bistatičkog radara.

Još jedan diskutirani eksperiment je *Mars Lander Radioscience* (LaRa) (Dehant et al. 2009). LaRa instrument bit će lansiran u sklopu ExoMars 2020 misije te ugrađen u sletač koji će boraviti na fiksnoj lokaciji na Marsovoj površini. LaRa će sadržavati radio transponder koji će razmjenjivati signal sa zemaljskim postajama za praćenje te će se iz njegovog Dopplerovog pomaka moći detektirati LaRina pozicija do na desetke centimetara. Zahvaljujući tome, bit će omogućena vrlo precizna karakterizacija brzine Marsove rotacije, kao i precesije i nutacije. Budući da je precesija inverzno proporcionalna momentu inercije, ovakav eksperiment bi mogao odgovoriti na pitanja o građi Marsove jezgre. Kako je PRIDE redovito demonstrirao sposobnost dostavljanja visokopreciznih Dopplerovih opservabli s orbitera oko Marsa, pokazao bi i vrijedno pojačanje za LaRu čiji rezultati ovise o količini vremena koje joj mogu dodijeliti ESA-ine i NASA-ine mreže praćenja.

6.5 Zaključak

Planetarni Radio Interferometrijski i Dopplerov Eksperiment (PRIDE) koristi metode i instrumentaciju dugobazične interferometrije (VLBI) u korist radioznanstvenih eksperimenata na svemirskim letjelicama i sletačima. Koristeći svjetske mreže teleskopa, PRIDE nudi najvišu preciznost u određivanju vektora stanja s bogatstvom primjena od gravimetrije i atmosferske znanosti do proučavanja koronalnih izbačaja mase.

U ovom radu raspravili smo planiranje PRIDE eksperimenta na primjeru opservacije dvaju orbitera na Marsu, od lociranja potencijalnih faznih kalibratora do određivanja pet promatračkih prilika za pojedine teleskope European VLBI Networka i Very Long Baseline Arraya. Ovakav eksperiment pridonijet će razumijevanju Marsovog sustava, kao i poboljšanju PRIDE-ove tehnike.

Primjer obrade podataka za PRIDE eksperiment proveden je na radiookultacijskoj studiji Marsove atmosfere. Izmjerena su svojstva signala Mars Express orbitera pri zalasku iza Marsovog horizonta, što je rezultiralo vertikalnim profilima refraktivnosti, gustoće, tlaka i temperature za stupac atmosfere do na manje od 10 kilometara od površine koristeći podatke s pet teleskopa.

Budućnost PRIDE-a istražena je u sklopu eksperimenta bistatičkog radara s JUpiter Icy moons Explorer (JUICE) misijom pri čemu bi letjelica odbila radioval od površine Jupiterovog mjeseca Europe. Antene EVN-a nude solidnu detektabilnost za ovakav

pothvat te bi mogle dati nove podatke o dielektričnim i reljefnim svojstvima površine. Dodatno, PRIDE-ovo promatranje ExoMars 2020 sletača na površini Marsa u sklopu Lander Radioscience (LaRa) eksperimenta mogao bi odgovoriti brojna pitanja o Marsovoj unutrašnjosti.

Uzevši u obzir da brojne primjene PRIDE-a ne zahtijevaju nikakvo dodatno financijsko i vremensko opterećenje na planiranje svemirskih misija, PRIDE će ostati moćan alat za planetarnu radio znanost u desetljećima u budućnosti.

Bibliography

Ao, C. O., Edwards, C. D., Kahan, D. S., et al. 2015, Radio Science, 50, 997

Bocanegra-Bahamón, T. M., Molera Calvés, G., Gurvits, L. I., et al. 2018, A&A, 609, A59

Born, M. & Wolf, E. 1999, Principles of Optics, 986

Broten, N. W., Legg, T. H., Locke, J. L., et al. 1967, Science, 156, 1592

Cahoy, K. L., Hinson, D. P., & Tyler, G. L. 2006, Journal of Geophysical Research: Planets, 111

Cain, D. L., Kliore, A. J., Seidel, B. L., & Sykes, M. J. 1972, Icarus, 17, 517

Cain, D. L., Kliore, A. J., Seidel, B. L., Sykes, M. J., & Woiceshyn, P. 1973, J. Geophys. Res., 78, 4352

Cui, J., Galand, M., Zhang, S. J., Vigren, E., & Zou, H. 2015, Journal of Geophysical Research: Planets, 120, 278

Dehant, V., Folkner, W., Renotte, E., et al. 2009, Planetary and Space Science, 57, 1050 , european Mars Science and Exploration Conference (EMSEC)

Duev, D. A., Molera Calvés, G., Pogrebenko, S. V., et al. 2012, A&A, 541, A43

Duev, D. A., Pogrebenko, S. V., Cimò, G., et al. 2016, A&A, 593, A34

Fjeldbo, G. 1964, Bistatic Radar Methods for Studying Planetary Ionospheres and Surfaces, SEL-64-025 (Department of Electrical Engineering, Stanford University.)

Fjeldbo, G. & Eshleman, V. R. 1968, Planet. Space Sci., 16, 1035

Fjeldbo, G., Kliore, A., & Seidel, B. 1970, Radio Science, 5, 381

Fjeldbo, G., Kliore, A. J., & Eshleman, V. R. 1971, AJ, 76, 123

Fjeldbo, G., Sweetnam, D., Brenkle, J., et al. 1977, J. Geophys. Res., 82, 4317

Folkner, W. M., Border, J. S., Nandi, S., & Zukor, K. S. 1993, Telecommunications and Data Acquisition Progress Report, 113, 22

Folkner, W. M., Williams, J. G., Boggs, D. H., Park, R. S., & Kuchynka, P. 2014, Interplanetary Network Progress Report, 196, 1

Garrett, M. A. 2004, ArXiv Astrophysics e-prints [astro-ph/0409021]

Gibney, E. 2016, Nature, 531, 288

Hinson, D. P., Asmar, S., Kahan, D., Akopian, V., & Maalouf, S. 2012, in AAS/Division for Planetary Sciences Meeting Abstracts, Vol. 44, AAS/Division for Planetary Sciences Meeting Abstracts #44, 214.13

Hinson, D. P., Asmar, S. W., Kahan, D. S., et al. 2014, Icarus, 243, 91

Hinson, D. P., Simpson, R. A., Twicken, J. D., Tyler, G. L., & Flasar, F. M. 1999, J. Geophys. Res., 104, 26997

Kinman, P. W. 1992, IEEE Transactions on Microwave Theory Techniques, 40, 1199

Kliore, A., Cain, D. L., Levy, G. S., et al. 1965, Science, 149, 1243

Kliore, A., Fjeldbo, G., & Seidel, B. 1970, Radio Science, 5, 373

Kliore, A., Fjeldbo, G., Seidel, B. L., & Rasool, S. I. 1969, Science, 166, 1393

Kliore, A. J., Cain, D. L., Fjeldbo, G., et al. 1972, Icarus, 17, 484

Kliore, A. J., Fjeldbo, G., Seidel, B. L., Sykes, M. J., & Woiceshyn, P. M. 1973, Journal of Geophysical Research, 78, 4331

Kolosov, M. A., Iakovlev, O. I., Iakovleva, G. D., et al. 1975, Cosmic Research, 13, 46

Kopeikin, S. M. & Schäfer, G. 1999, Phys. Rev. D, 60, 124002

Lindal, G. F., Hotz, H. B., Sweetnam, D. N., et al. 1979, J. Geophys. Res., 84, 8443

Linscott, I., Protopapa, S., Hinson, D. P., et al. 2016, in AAS/Division for Planetary Sciences Meeting Abstracts, Vol. 48, AAS/Division for Planetary Sciences Meeting Abstracts #48, 213.04

Molera Calvés, G. 2017, American Geophysical Union

Noguchi, K. 2012, in European Planetary Science Congress 2012, EPSC2012–462

Pätzold, M., Tellmann, S., Häusler, B., et al. 2005, Science, 310, 837

Petrov, L. 2017, Radio Fundamental Catalog, version `rfc2017c`

Pätzold, M., Häusler, B., Tyler, G., et al. 2016, Planetary and Space Science, 127, 44

Rasool, S. I., Hogan, J. S., Stewart, R. W., & Russell, L. H. 1970, Journal of Atmospheric Sciences, 27, 841

Ryle, M. 1961, in Large Radio-Telescopes, 85

Savich, N. A., Samovol, V. A., Vasilyev, M. B., et al. 1976, NASA Special Publication, 397

Schmidt, R. 2003, Acta Astronautica, 52, 197

Simpson, R. A. 1993, IEEE Transactions on Geoscience and Remote Sensing, 31, 465

Simpson, R. A. & Tyler, G. L. 1981, Icarus, 46, 361

Tellmann, S., Pätzold, M., Häusler, B., Hinson, D. P., & Tyler, G. L. 2013, Journal of Geophysical Research: Planets, 118, 306

Thompson, A. R., Moran, J. M., & Swenson, Jr., G. W. 2017, Interferometry and Synthesis in Radio Astronomy, 3rd Edition

Tyler, G. L., Balmino, G., Hinson, D. P., et al. 2001, J. Geophys. Res., 106, 23327

Vasil'Ev, M. B., Vyshlov, A. S., Kolosov, M. A., et al. 1975, Kosmicheskie Issledovaniia, 13, 48

Weiner, S. L. & Withers, P. 2013, AGU Fall Meeting Abstracts, P21A

Willis, N., Griffiths, H., & Davis, M. 2007, Advances in Bistatic Radar, Electromagnetics and Radar (Institution of Engineering and Technology)

Wilson, T. L., Rohlfs, K., & Hüttemeister, S. 2009, Tools of Radio Astronomy (Springer-Verlag)

Zhang, S. J., Cui, J., Guo, P., et al. 2015, Advances in Space Research, 55, 2177